Effect of 50 T Pulsed Magnetic Field on Different Microorganisms

Barbosa-Cánovas, G.V., Washington State Univ., Biological Systems Engineering
San Martin, F., Washington State Univ., Biological Systems Engineering
Harte, F., Washington State Univ., Biological Systems Engineering
Swanson, B.G., Washington State Univ., Food Science and Human Nutrition

The use of magnetic fields to inactivate microorganisms has been suggested as a nonthermal technology to achieve safe foods. Previous work by this group showed that an 18 T static or pulsed magnetic field did not have any inactivation effect on *Escherichia coli* nor *Saccharomyces cerevisiae* suspended in nutrient broth or buffer solution. The objective of the present work was to study if a pulsed field of higher intensity causes any inactivation on *Escherichia coli*, *Saccharomyces cerevisiae*, *Bacillus subtilis,* or *Listeria innocua*.

Cryogenic vials containing 2 mL of the culture each were introduced in the center bore of a capacitor driven short pulse magnet available at LANL. Each vial was subjected to 1, 2, or 3 pulsed magnetic fields of 50 T. All vials were submerged in liquid nitrogen during treatments. Results for treated samples did not show any inactivation effect when compared to control samples that were kept frozen but without exposure to the magnetic field (Fig. 1). It was concluded that pulsed magnetic fields of 50 T were not effective in inactivating the microorganisms in frozen state.

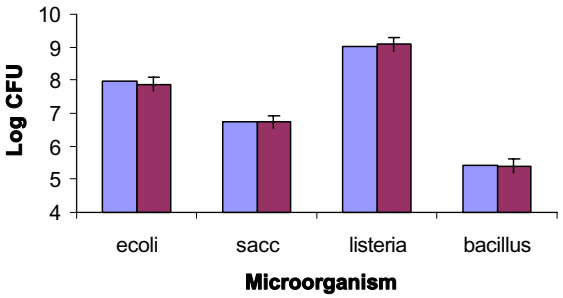

Figure 1. Inactivation effect of three 50 T pulses on different microorganisms (error bars are confidence intervals α).

The Regulatory Domain of the Myosin Head Behaves as a Rigid Lever

Baumann, B.A.J., FSU, Molecular Biophysics
Hambly, B.D., Univ. of Sydney, Australia, Pathology
Hideg, K., Univ. of Pecs, Hungary, Institute of Organic and Medicinal Chemistry
Fajer, P.G., NHMFL/FSU, Biological Sciences and Institute of Molecular Biophysics

The regulatory domain of the myosin head is believed to serve as a lever arm that amplifies force generated in the catalytic domain and transmits this strain to the thick filament. The lever arm itself can be either passive, or may have a more active role storing some of the energy created by hydrolysis of ATP. A structural correlate which might distinguish between the two possibilities is the stiffness of the domain in question. To this effect, we have examined the motion of the proximal (ELC) and distal (RLC) subdomains of the regulatory domain in reconstituted myosin filaments. Each subdomain was labeled with a spin label at a unique cysteine residue, cys-136 of ELC or cys-154 of mutant RLC, and its mobility was determined using saturation transfer electron paramagnetic resonance spectroscopy. The mobility of the two domains was similar; the correlation time for ELC was 17 μs, and 22 μs for RLC. Additionally, following a two-fold change of the global dynamics of the myosin head, effected by decreasing the interactions with the filament surface (or the other myosin head), the coupling of the intra-domain dynamics remained unchanged. These data suggest that the regulatory domain of the myosin head

acts as a single mechanically rigid body, consistent with the regulatory domain serving as a passive lever.

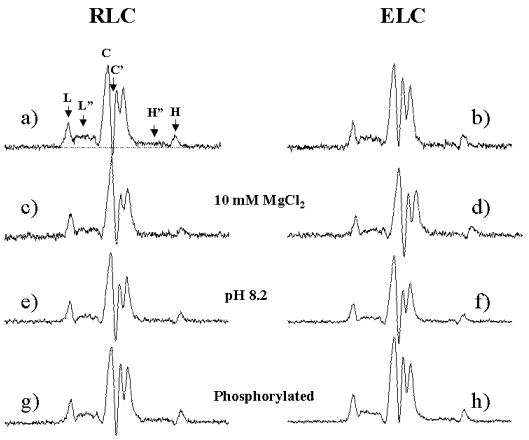

Figure 1. ST-EPR spectra of InVSL labeled RLC and ELC myosin filaments: RLC (a) and ELC (b) at pH 7.0; in 10 mM $MgCl_2$ (c) and (d) RLC and ELC, respectively; pH 8.2 (e) and (f); with RLC phosphorylated (g) and (h). A decrease in intensity of L" (normalized to the intensity at L) indicates a lower τ_{eff} and a higher mobility.

MR Microimaging Studies of Mouse Brains For Generation of a Web-Based Atlas

Benveniste, H., Duke Univ., Anesthesiology
Plant, D., UF McKnight Brain Institute
Hedges, D., UF McKnight Brain Institute
Blackband, S., UF McKnight Brain Institute/UF, Neuroscience/NHMFL

A new collaboration has developed this year with Dr. Helene Benveniste at Duke University. Dr. Benveniste is funded by the NIH to develop a web-based probabilistic atlas of the mouse brain. The purpose of this project is to produce a 3D atlas of the mouse brain using MR microscopy as an aid for functional genomics. Suitable MR "stains" (relaxation and diffusion contrast) will be employed.

In order to be the most effective for functional genomics, the highest possible resolution 3D data sets are required to form the atlas. In collaboration with Dr. Benveniste, we are exploring the utility of the 750 MHz for generating this map. Fig. 1 shows

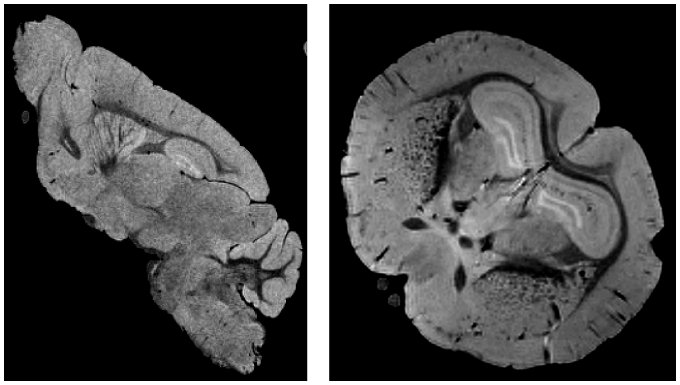

Figure 1. Example slices from a gradient echo 3D data set with TR=150 ms and TE=7.4 ms, generating a 47 μm isotropic spatial resolution in 2 hours 43 minutes.

example data sets after optimizing 3D gradient echo imaging at 750 MHz using the commercial rf probes. Explorations on the appropriate "stain" to use will be carried out separately at Dr. Al Johnson's facility at Duke. If the 750 MHz proves superior for these studies, as our early results suggest, then the mouse brain atlas may be generated by scanning samples in the Advanced Magnetic Resonance Imaging and Spectroscopy (AMRIS) facility using the stains determined by Dr. Johnson.

Acknowledgements: This work was supported by the NHMFL, the NIH, and the UF McKnight Brain Institute.

NMR Microscopy and Spectroscopy of Single Cells ◤IHRP◢

Blackband, S.J., UF McKnight Brain Institute/UF, Neuroscience/NHMFL
Grant, S., Univ. of Chicago, Bioengineering
Thelwall, P., UF McKnight Brain Institute
Webb, A., Univ. of Illinois, Electrical and Computer Engineering
Gibbs, S., NHMFL/FAMU-FSU College of Engineering
Plant, D., UF McKnight Brain Institute
Mareci, T., UF McKnight Brain Institute/UF, Biochemistry/NHMFL

Studies on single neurons isolated from the marine gastropod, *Aplysia californica,* have continued through the third and final year of an NIH grant. Using

microcoils developed by Drs. Webb and Grant, the first spatially localized ^{1}H spectra of the osmolyte and metabolite content of a single cell have now been published.[1] Improvements in SNR are required so that intracellular heterogeneity can be addressed. Towards these ends, the first microcoils for use on the new 750 MHz wide bore at UF have been constructed and are being evaluated.

The interpretation of diffusion signals in tissues has been problematic, with non-monoexponential diffusion curves implying compartmentation within the tissues. The origins of this compartmentation are unclear, but may reflect to some degree intra/extracellular compartments. To shed further light on these issues, we have examined the diffusion coefficient (D) of water in single neurons from *Aplysia,* and have observed non-monoexponential D within the cytoplasm (SNR limitations have limited the interpretation of nuclear signals due to volume averaging at the low spatial resolution needed to get good diffusion curves), indicating multiple water compartments within the cell (2,3). Models are under development to determine how these observations will aid in the interpretation of diffusion in tissues. The implementation of these experiments on the 750 MHz will help improve the SNR and improve localization to the cell nucleus.

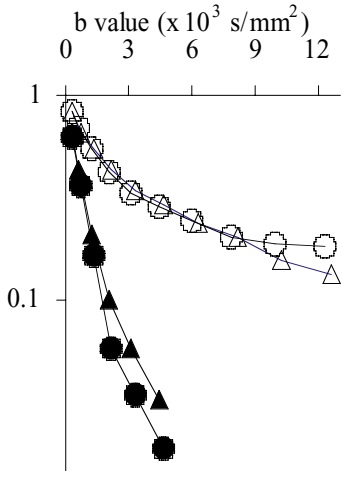

Figure 1. Normalized diffusion curves measured in the cytoplasm (open symbols) and nucleus (filled symbols) of a typical cell. Data were acquired using diffusion times of 10 ms (triangles) and 18 ms (circles). Note the significant difference in ADCs of cytoplasm and nucleus and the minimal influence of diffusion time. It is clear from these semi-log plots that curves for the cytoplasm are not monoexponential.

Acknowledgements: This work was supported by the IHRP of the NHMFL, the NIH, and the UF McKnight Brain Institute.

[1] Grant, S.C., *et al*., Magn. Reson. Med., **44**, 19-22 (2000).
[2] Grant, S.C., *et al*., Proc. of the ISMRM, Denver (2000).
[3] Grant, S.C., *et al*., submitted to, Magn. Reson. Med. (2000).

NMR Microscopy of Isolated Perfused Brain Slices

Blackband, S.J., UF McKnight Brain Institute/UF, Neuroscience/NHMFL
Bui, J.D., UF, Physiology
Roper, S., UF, Neurosurgery
Thelwall, P., UF McKnight Brain Institute
Phillips, M.I., UF McKnight Brain Institute

Studies continue examining the NMR characteristics of isolated perfused brain slices as a model of tissues. Last year, we described basic studies illustrating the compartmental nature of diffusion signals in the slices and how these change with perturbations in a way that implicate changes in intra and extracellular compartmentation. Such information has significant clinical potential. Since that time, we have used Gd-DTPA to confirm the origins of the cellular compartmentation.[1] Similar studies on isolated perfused heart tissue slices, have been accepted subject to minor modifications.[2]

To explore the clinical utility and significance of these studies, we have most recently extended these studies to the examination of isolated fixed human brain slices on the new 750 MHz instrument. Fig. 1 shows one of the first images of such a slice. Procedures are under development to facilitate the study of *in vivo* isolated human brain slices.

Acknowledgements: This work was supported by the NIH and the UF McKnight Brain Institute.

[1] Buckley, D.L. *et al.,* Magn Reson Med, in press (2000).
[2] Forder, *et al.,* submitted Am J Physiol (2000).

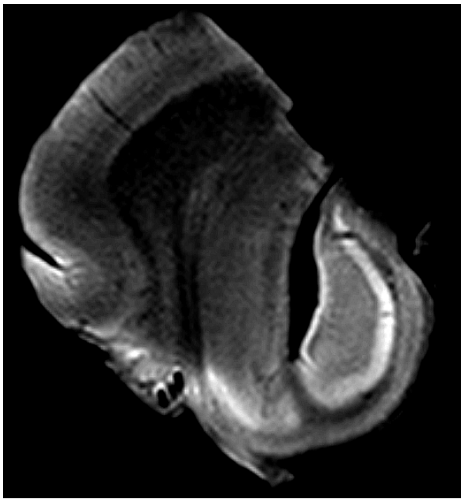

Figure 1. Diffusion weighted MR microimage of an isolated slice of human brain tissue (unperfused) obtained on our new 750 MHz instrument. The hippocampal tissue was excised from an epilepsy patient. Resolution = 0.1 x 0.1 x 0.4 mm, b = 2000 s/mm^2, acquired in 21 minutes.

Functional and Spectroscopic Studies of an FHC Mutation in Motif X of Cardiac Myosin Binding Protein-C

Brown, L., Univ. of Sydney, Pathology
Singh, L., Univ. of Sydney, Pathology
Sale, K., NHMFL/FSU, Biology
Yu, B., Univ. of Sydney, Molecular and Clinical Genetics and Medicine
Trent, R., Univ. of Sydney, Molecular and Clinical Genetics and Medicine
Fajer, P.G., NHMFL/FSU, Biology and Molecular Biophysics
Hambly, B.D., Univ. of Sydney, Pathology

Familial hypertrophic cardiomyopathy is an autosomal dominant genetic disorder associated with sudden death in young adults, caused by mutations in cardiac sarcomeric proteins. One such mutation is a six amino acid duplication of residues 1248-1253 in the immunoglobulin domain Motif X of cardiac myosin binding protein-C. Motif X binds the myosin rod and titin.

Here, we investigate the structural and functional alteration in this mutant MyBP-C domain to understand how sarcomeric dysfunction may occur at the protein level. The cDNA encoding Motif X was cloned, mutated, and expressed as wild-type and mutant proteins in a bacterial expression system. Circular dichroism spectroscopy was used to confirm that the normal and mutant Motif X exhibited a high β-content, as predicted for immunoglobulin domains. Thermal denaturation curves showed that Motif X unfolded with at least two structural transitions, with the first transition occurring at 63^o in the wild-type, but at 40^o in the mutant, consistent with the mutant being slightly structurally less stable. Sedimentation binding studies with myosin filaments showed no significant difference in binding between the normal and the mutant Motif X. Molecular modeling of this insertion onto an homologous IgI structure (telokin) revealed that the duplicated residues lie within the F strand of the immunoglobulin fold, on a surface of Motif X distant from residues previously implicated in myosin binding.[1] Taken together, these data suggest that the Motif X mutation may interfere with other, as yet unidentified functional interactions.

[1] Miyamoto, C., *et al*., J. Musc. Res. Cell Motil., **20**, 703, (1999).

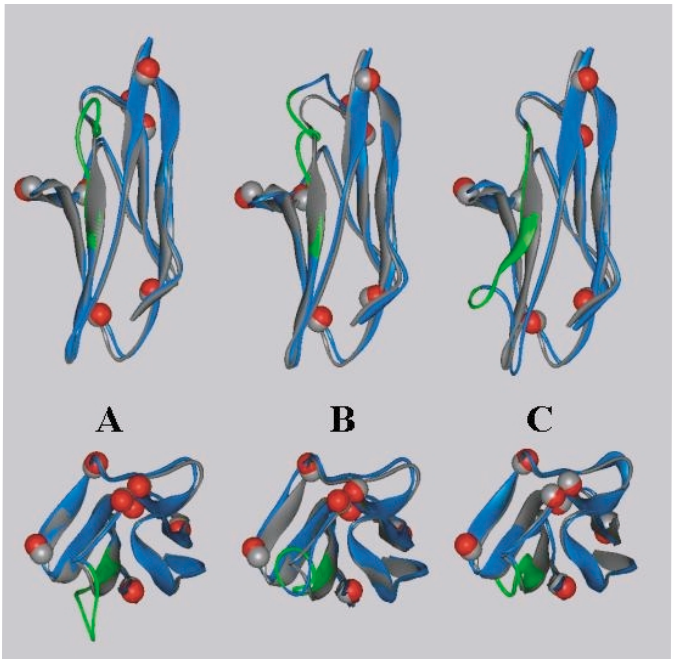

Figure 1. Molecular models of Motif X wild type and mutant structures. Overlays of the wild type and mutant structures build by homology building: (a) mutant built from the Motif X wild type starting at N-terminus; (b) Motif X mutant and wild type modeled from telokin structure; (c) as in (a) but threading from the C-terminus.

Independent Movement of Regulatory and Catalytic Domains of Myosin Heads Revealed by Phosphorescence Anisotropy

Brown, L.J., Univ. of Sydney, Pathology, NHMFL/FSU
Klonis, N., Univ. of Melbourne, Biochemistry and Molecular Biology
Sawyer, W.H., Univ. of Melbourne, Biochemistry and Molecular Biology
Fajer, P.G., NHMFL/FSU, Biological Sciences
Hambly, B.D., Univ. of Sydney, Pathology

Inter- and intradomain flexibility of the myosin head was measured using phosphorescent anisotropy of selectively labeled parts of the molecule. Whole myosin and the myosin head, subfragment-1 (S1), were labeled with eosin-5-iodoacetamide on the catalytic domain, (cys 707), and on two sites on the regulatory domain (cys 177 on the essential light chain, and cys 154 on the regulatory light chain).

Phosphorescence anisotropy was measured in soluble S1 and myosin, with and without F-actin, as well as in synthetic myosin filaments. The anisotropy of the former were too low to observe differences in the domain mobilities, including when bound to actin. However, this was not the case in the myosin filament. The final anisotropy of the probe on the catalytic domain was 0.051 which increased for probes bound to the essential and regulatory light chains to 0.085 and 0.089, respectively. These differences can be expressed in terms of a "wobble in cone" model, suggesting various amplitudes. The catalytic domain is least restricted, with a 40° ± 5° half-cone angle, whereas the essential and regulatory light chain amplitude is less than 28°. These data demonstrate the presence of a point of flexibility between the catalytic and regulatory domains.

The presence of the "hinge" between the catalytic and regulatory domains, with a rigid regulatory domain, is consistent with both the "swinging lever arm" and "Brownian ratchet" models of force generation. However, in the former case, there is a postulated requirement for the hinge to stiffen to transmit generated torque associated by nucleotide hydrolysis and actin binding.

Acknowledgements: Research was sponsored by the NHMRC of Australia, National Science Foundation NSF-IBN-9808708, NHMFL IHRP 5024 and the American Heart Association GIA-9950424N.

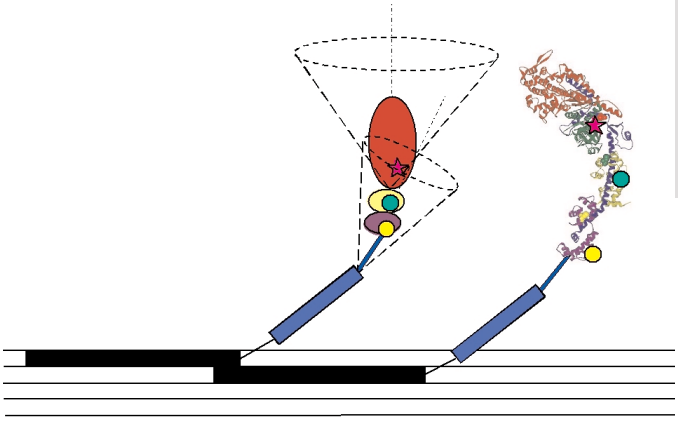

Figure 1. A model of myosin head motion. The estimated half-cone angle for the catalytic and regulatory domains in filaments. The catalytic domain amplitude is 40° ± 5° and the regulatory domain is 28° ± 7° (28° ± 9° for ELC and 27° ± 6° for RLC).

Gas-Phase Hydrogen Deuterium Exchange of Positively Charged Mononucleotides by Use of Fourier Transform Ion Cyclotron Resonance Mass Spectrometry

Church, K.G., Louisiana State Univ., Chemistry
Limbach, P.A., LSU, Chemistry
Freitas, M.A., NHMFL
Marshall, A.G., NHMFL/FSU, Chemistry

The gas-phase structures of protonated (deoxy)nucleoside-5'- and 3'-monophosphates (mononucleotides) have been examined by the use of gas-phase hydrogen/deuterium (H/D) exchange and high-field Fourier transform ion cyclotron resonance mass spectrometry (FTICRMS). These nucleotides were reacted with three different deuterating reagents: ND_3, D_2O and D_2S, of which ND_3 was the most effective. All mononucleotides fully exchanged their labile hydrogen for deuterium with ND_3 with the exception of deoxycytidine-3'-monophosphate, deoxyadenosine-5'-monophosphate, adenosine-5'-monophosphate and adenosine-3'-monophosphate.

Incomplete exchange for these four mononucleotides is attributed to either intermolecular hydrogen bonding or steric hindrance. Semi-empirical calculations demonstrate the presence of hydrogen bonding upon protonation of the mononucleotide leading to incomplete H/D exchange. The results also suggest that (deoxy)guanosine monophosphates are protonated at N7 rather than N3, although N3 is the site of highest proton affinity. H/D exchange rates differed between the deoxymononucleotides and the ribomononucleotides, suggesting that the 2'-OH group plays an important role in the exchange process. Comparison of the gas-phase H/D exchange kinetics of mononucleotides with the corresponding nucleosides suggests that the phosphate group facilitates the exchange of the mononucleotides when D_2O is used as a deuterating reagent but not when ND_3 is used. However, H/D exchange kinetics indicate that all mononucleotides first exchange labile hydrogens associated with the sugar-phosphate moiety regardless of the identity of the exchange reagent. The present results provide the most detailed mechanistic analysis to date for proton exchange behavior of positively charged gas-phase RNA and DNA mononucleotides.

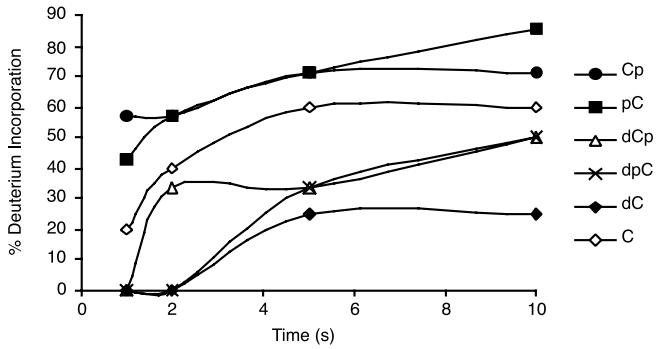

Figure 1. Plots of deuterium incorporation vs. time for a) guanosine-5'-monophosphate (pG), b) guanosine-3'-monophosphate (Gp), c) deoxycytidine-3'-monophosphate (dCp), d) deoxyadenosine-5'-monophosphate (dpA), e) deoxyadenosine-3'-monophosphate, and f) adenosine-5'-monophosphate after a 600 second reaction period with ND_3.

Acknowledgements: The authors thank Professor David Dearden (Brigham Young University) for providing the KinFit program. Financial support of this work was provided by the NSF National High Field FT-ICR Facility (to A.G.M.) (CHE-94-13008, CHE-93-22824), the National Institutes of Health (to P.A.L.) (HG01777), FSU, and Louisiana State University.

[1] Green-Church, K., *et al.*, "Gas-Phase Hydrogen Deuterium Exchange of Positively Charged Mononucleotides by Use of Fourier Transform Ion Cyclotron Resonance Mass Spectrometry," J. Am. Soc. Mass Spectrom., **12,** 0000-0000 (2001).

Biophysical Studies of MARCKS: Implications for Neuroplasticity

Edison, A.S., NHMFL/UF, Biochemistry
Bubb, M.R., UF, Medicine
Lenox, R.H., Univ. of Pennsylvania, Psychiatry

Myristoylated alanine-rich protein kinase C substrate (MARCKS) is a prominent protein substrate for protein kinase C that binds calmodulin in a calcium-dependent manner, binds and crosslinks filamentous actin, and is implicated in cellular processes associated with cytoskeletal restructuring, e.g., transmembrane signaling and neurotransmitter release. A highly conserved phosphorylation site domain (PSD) is the binding site for both actin and calmodulin, and may also bind directly to plasma membrane through acidic phospholipids. Considerable work has demonstrated a role for MARCKS in long term events in cell function that are associated with alteration in actin-membrane plasticity in the brain. In particular, the regulation of MARCKS expression is involved with brain development, neuronal regeneration, and represents a molecular target in the brain for the action of mood stabilizers such as lithium in the treatment of manic-depressive illness.

Last year, we reported that we determined that phosphorylation of MARCKS-PSD produced a structure that is more compact than the non-phosphorylated version.[1] The NMR results lead to the following hypothesis: Phosphorylation-induced

conformational changes in MARCKS-PSD regulate actin cross-linking. In particular, fully extended (non-phosphorylated) MARCKS-PSD cross-links actin, because it contains two accessible acting-binding sites. Phosphorylated MARCKS-PSD cannot bind two actin filaments because of steric clashes and thus cannot cross-link actin. Over the previous year, we have tested the hypothesis by conducting a series of actin-binding studies with various truncated forms of MARCKS-PSD.[2] These studies support the conformational hypothesis generated by the initial NMR analysis and will be published shortly. We are also developing a FRET-based measurement strategy to determine the end-to-end distances of MARCKS-PSD as a function of phosphorylation. These distances will be used in conjunction with shorter range NMR distance restraints in molecular modeling.

Acknowledgements: This work was supported by the NHMFL and the UF McKnight Brain Institute.

[1] Bubb, *et al.,* JBC 274, 36472 (1999).
[2] Edison, A.S., *et al.,* Society for Neuroscience, New Orleans, LA, Nov 4-9 (2000).

Structural and Dynamical Studies of IA-3, a Potent Yeast Proteinase A Inhibitor

Edison, A.S., NHMFL/UF, Biochemistry
Green, T., UF, Biochemistry and Molecular Biology
Dunn, B., UF, Biochemistry and Molecular Biology
Kay, J., Cardiff Univ., UK, Biosciences
Wlodawer, A., National Cancer Institute

Proteases are attractive targets for drug design against microbial pathogens, because the proteases are often essential to the life cycle of the pathogen and are sometimes directly related to acute damage in the host. Moreover, proteases from different species often have slightly different properties, allowing for the development of highly selective inhibitors. This project is focused on elucidating the structural features of a 68 amino acid yeast protein, IA-3, which is a potent inhibitor of yeast proteinase A (YprA). IA-3 binds to YprA with exceptional affinity (K_D is sub-nanomolar) and specificity. An x-ray crystal structure of the IA-3/YprA complex has recently been solved in Wlodawer's laboratory,[1] and in that structure, IA-3 forms a near-perfect alpha-helix in its first 33 amino acids. The C-terminal domain was not observed in the electron density. Until this finding, all protease inhibitors were thought to bind in extended conformations.

Using NMR, we have completely assigned the resonances of IA-3 in solution using triple resonance techniques (Fig. 1). The chemical shifts, H/D exchange, 15N-1H NOEs, and lack of 1H-1H NOEs all demonstrate that IA-3 is completely unstructured in solution. However, the NMR sample was found to be completely active as a YprA inhibitor. 15N-HSQC data show a dramatic change in conformation from the free to the YprA-bound IA-3. We are nearly complete in the analysis of IA-3 in saturating amounts of trifluoroethanol (TFE) to see which regions of the molecule are most susceptible to helical transitions. This work will is in preparation for publication.

Acknowledgements: This work was supported by the NHMFL, the NIH, and the UF McKnight Brain Institute.

[1] Li, *et al.,* Nature Structural Biology, **7,** 113-117 (2000).

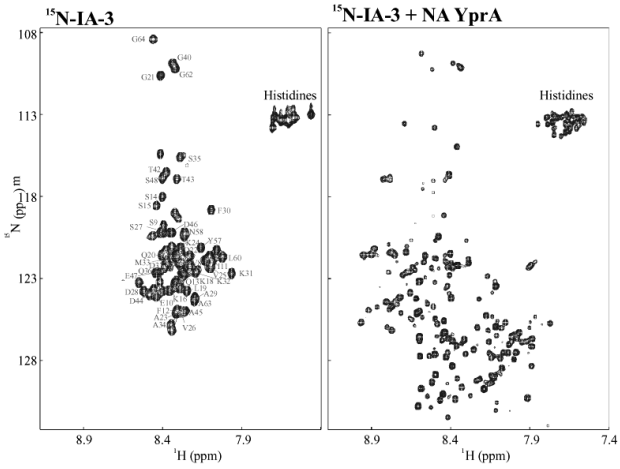

Figure 1. ^{15}N HSQC spectra of IA-3 alone (left) and in complex with YprA (right). The sample on the left is unfolded and completely active.

Structural Studies of Mutacin 1140

Edison, A.S., NHMFL/UF, Biochemistry
Smith, L., UF, Neuroscience
Hillman, J., UF, Oral Biology
Novak, J., Univ. of Alabama, Microbiology and Oral Biology

Mutacin 1140 is a naturally occurring lantibiotic produced by the bacterium *Streptococcus mutans*. Lantibiotics are ribosomally produced antibiotics that contain a large number of post-translational modifications, such as dehydrated amino acids and thioether bridges. The thioether bridges form between cysteine residues and modified serine and threonine residues. Mutacin 1140 has exceptional antibiotic activity against a broad range of Gram-positive bacteria.

This year we have published the covalent structure of mutacin 1140.[1] This was challenging, due to the numerous post-translational modifications in the molecule. We have also solved the 3D structure of mutacin 1140 by NMR. Although it is a small peptide (21 amino acids), mutacin 1140 is remarkably rigid due to 4 rings and several amino acids with alpha-beta double bonds (Fig. 1). The 3D structure is in agreement with a substantial amount of chemical data, and we are in the process of using the structure to generate a model for the mechanism of action of this important antibiotic.

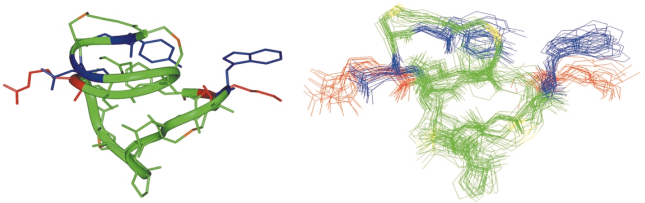

Figure 1. 3D NMR structures of mutacin 1140. Shown on the right is a superposition of 20 energy minimized structures from a 100 ps restrained molecular dynamics simulation in explicit acetonitrile solvent. The left is a ribbon diagram of the average structure. Full details of the calculations will be published later this year.

Acknowledgements: This work was supported by the NHMFL, the NIH, and the UF McKnight Brain Institute.

[1] Smith, L., *et al*., European Journal of Biochemistry**, 267** (23), 6810-6816 (2000).

Structure/Function Relations of Neuropeptides and Neuropeptide Precursor Proteins

Edison, A.S., NHMFL/UF, Biochemistry
Zachariah, C., UF, Biochemistry and Molecular Biology
Thomas, S., UF, Biochemistry and Molecular Biology
Espinoza, E., UF, Biochemistry and Molecular Biology

We are using NMR to study the structural properties of a large family of neuropeptides called FMRFamide-like peptides (FLPs). There are several hundred FLPs throughout the animal kingdom, and some organisms have more than 50 different (but closely related) FLPs. Neuropeptides have 3 main "states" *in vivo*: (1) They are expressed as longer precursor proteins that often contain multiple copies of peptides. (2) They exist as free, fully processed peptides. (3) They bind to and activate different types of receptors.

Recently, we showed that a family of related peptides with single changes in amino acid sequence had large changes in the amount of reverse turn in solution. As reported last year, these changes are inversely correlated with the receptor binding affinity, suggesting that the turns inhibited access of the peptides to the receptor. The NMR work has now been confirmed computationally with Monte Carlo simulated annealing calculations.[1] We also completed a statistical survey of FLPs to guide future structural studies.[2]

In the area of FLP precursor processing, we have used NMR to study two similar synthetic peptides which contain two unprocessed FLPs

with an intact processing site. The peptides are identical except for a single amino acid insertion (GDPFLRFGRGDPFLRFamide vs. GDPFLRFGR-GDSPFLRFamide). The single amino acid change leads to very large conformational changes and different biological functions. This work has been submitted for publication.

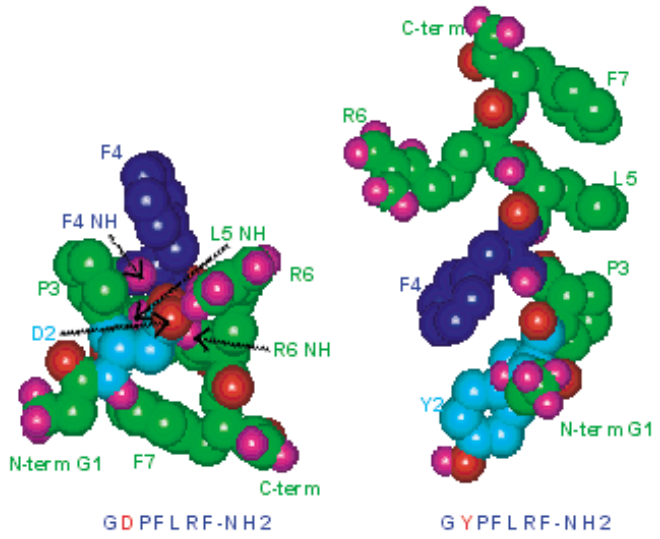

Figure 1. Lowest energy structures from Monte Carlo simulated annealing calculations of two similar neuropeptides. Both structures are consistent with previous NMR data and are described in Edison and Carlacci (2000).

Acknowledgements: This work was supported by the NSF, the NHMFL, and the UF McKnight Brain Institute.

[1] Carlacci, L., *et al.,* Proteins: Structure, Function, and Genetics, **40**, 367-377 (2000).
[2] Espinoza, E., *et al.,* Molecular Neurobiology (2001), in press.

MR Biexponential Diffusion Tensor Imaging of Isolated Rat Hearts

Forder, J., Univ. of Alabama, Medicine
Hsu, E., Duke Univ., Biomedical Engineering
Buckley, D.L., Univ. of Manchester, England, Imaging Science & Biomedical Engineering
Bui, J.D., UF, Physiology
Blackband, S., UF McKnight Brain Institute/UF, Neuroscience/NHMFL

In other studies on isolated heart slices, we have demonstrated the multicompartmental nature of the diffusion signals. However, studies of heat tissue is complicated by the anisotropy of the diffusion, necessitating the implementation of diffusion tensors in these tissues in a similar fashion to diffusion tensor studies in spinal cord tissue.

In collaboration with Dr. Hsu at Duke, and Dr. Buckley in England, Dr. Forder has led studies on developing multicompartmental diffusion tensor mapping in isolated hearts. A preliminary account of this work was presented at the ISMRM,[1] and after further evaluation, a publication is under review.[2] Fig. 1 shows an example of the calculated diffusion maps that can be generated, where the change in color across the heart wall represents the change in the fibre orientation going from the epi to endocardium. Although the biexponential model provides a preliminary understanding, a more complete model is required and is under development. Nevertheless, these preliminary findings provide further insight into the distribution of water in the myocardium.

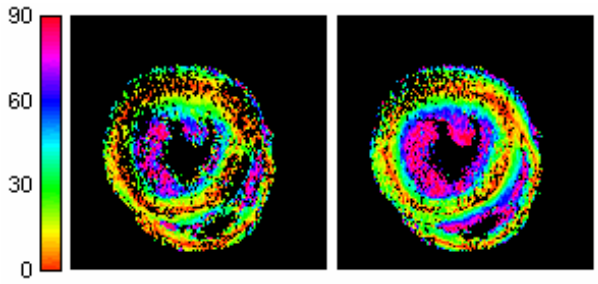

Figure 1. Helix angle maps of the primary eigenvectors of the fast (left) and slow (right) diffusion compartments in one heart.

Acknowledgements: This work was supported by the NHMFL, the NIH, and the UF McKnight Brain Institute.

[1] Hsu, E., *et al.*, Proc. ISMRM, Denver (2000).
[2] Hsu, E., *et al.*, submitted, Magn Reson Med (2000).

Competitive Binding to the Oligopeptide Binding Protein, OppA: In-Trap Cleanup in an FT-ICR Mass Spectrometer

Freitas, M.A., NHMFL
Hendrickson, C.L., NHMFL
Marshall, A.G., NHMFL/FSU, Chemistry
Rostom, A.A., Oxford University, New Chemistry Laboratory
Robinson, C.V., Oxford University, New Chemistry Laboratory

Here, we demonstrate that gentle infrared laser heating can remove unwanted buffer adducts from a gas-phase protein complex without dissociating the complex itself. Specifically, non-covalent complexes of the oligopeptide-binding protein, OppA, bound to either $(Ala)_3$ or LysTrpLys were electrosprayed from aqueous buffer solution into a 9.4 T Fourier transform ion cyclotron resonance mass spectrometer. In addition to the intact complexes, several additional buffer adduct species were produced under the conditions of the experiment. Irradiation of the trapped ion population with a continuous-wave infrared CO_2 laser at relatively low power (2.5 W) for 1 s dissociated the buffer adducts but retained the intact protein:peptide complexes. Adduct-free complex(es) were then readily identified, and signal-to-noise ratio also increased by an order of magnitude because the same number of protein ions are distributed over fewer species. Higher IR power (5 W for 1 s) dissociated the adduct-free complex(es) without internal fragmentation. The present in-trap clean-up technique may prove especially useful for identifying and screening the combinatorial library ligands **most strongly bound to a receptor in the gas phase.**

Acknowledgements: We thank Jeremy Tame for the OppA protein, as well as John P. Quinn and Daniel McIntosh (NHMFL) for their technical expertise and helpful discussions. This work was supported by NSF (CHE-93-22824), the NSF National High Field FT-ICR Facility (CHE-94-13008), FSU, and the NHMFL. Adam Rostom acknowledges support from the BBSRC and Zeneca Pharmaceuticals. Carol Robinson acknowledges support from the Royal Society and the Oxford Centre for Molecular Sciences.

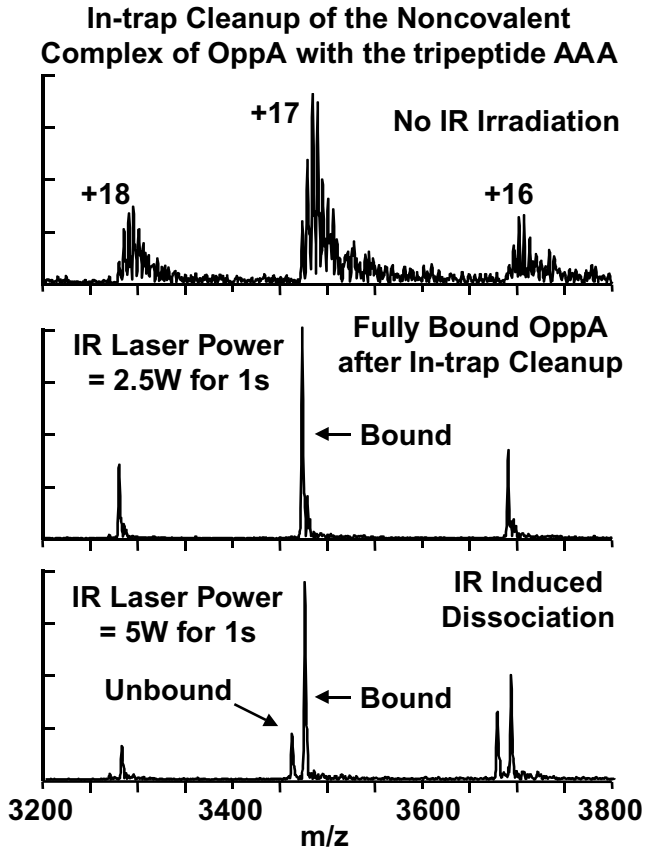

Figure 1. Electrospray ionization 9.4 T FT-ICR mass spectra illustrating in-trap cleanup of the oligopeptide binding protein, OppA:$(Ala)_3$ complex by application of infrared radiation from a CW CO_2 laser. Note the presence of several buffer adducts (top, no irradiation), their elimination by mild IR heating (middle, 2.5 W for 1 s), and photodissociation of the complex by stronger IR heating (bottom, 5 W for 1 s).

[1] Freitas, M.A., *et al.*, J. Am. Soc. Mass Spectrom., **11**, 1023-1026 (2000).

Prediction of Alpha-Helical Transmembrane Protein in *Mycobacterium Tuberculosis* Genome

◤IHRP◢

Gao, F., NHMFL
Cross, T.A., NHMFL/FSU, Chemistry

The genome sequencing projects provide new opportunities and challenges to the fields of structural biology and molecular biophysics. A new field, structural genomics, has emerged to focus on the large-

scale analysis of protein structures and functions. One of the projects in our lab is to organize a large, cooperative pilot study in structural gemonics focusing on membrane proteins. These proteins are responsible for transmembrane signaling, energy transduction, and ion and metabolite transport. More than 90% of the neuroscience drug targets are membrane proteins. Despite their importance and the need for structure to understand their function, few high-resolution structures are available, because they are particularly difficult to structurally characterize.

One of the basic issues that arise in structural genomics is the ability to predict the subcellular location of proteins that are deduced from genome sequence. Basic dogma holds that the primary sequence of a protein alone can be used to predict higher orders of protein structure. This basic doctrine can be applied to membrane sequences for accurate prediction of their topology. A large number of proteins in a genome encodes integral membrane protein. Most of them have transmembrane alpha helices. Knowledge of the presence and the exact number of helices is important for functional annotation and target selection for structural studies.

Using several prediction programs available, we have identified potential integral membrane proteins with alpha transmembrane helices in *Mycobacterium tuberculosis,* whose genome had been completely sequenced. The genome of this bacterium comprises 4.4 million base pairs. The size is only surpassed by *Escherichia coli* in the list of bacterial genomes completed to date. There are 3924 genes in the open reading frame. Among them, 1165 were found to have transmembrane alpha helical domains, about 30% of the total proteins in the genome. The number of transmembrane helices range from 1 to 18. Fig. 1 is the prediction result of one of the genes (Rv1217c) using TMHMM model. It shows the protein has 12 transmembrane alpha helices. These membrane proteins are further classified into functional groups. The result of the study has provided candidate membrane proteins for structural characterization in a large-scale approach.

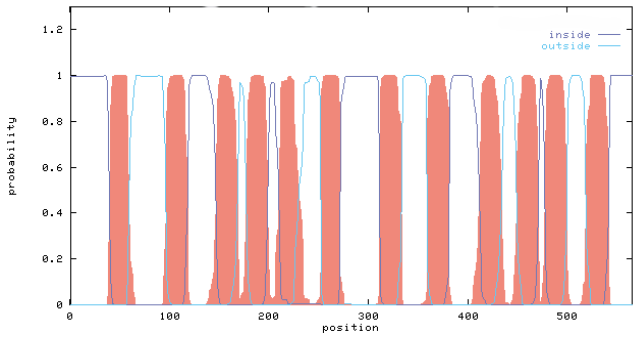

Figure 1. Prediction result of one of the genes (Rv1217c) using TMHMM model. The plot shows the probabilities of inside/outside/TM helix portion of the protein. The transmembrane portion is shown as columns. The inside/outside portions are shown as solid/dash line.

Structural Mapping of *Escherichia coli* Lactose Permease Using ^{19}F Solid State NMR Spectroscopy ◤IHRP◢

Gao, F., NHMFL/Univ. of California-Los Angeles, Physiology, and Howard Hughes Medical Institute
Fu, R., NHMFL
Wang, J., NHMFL
Kaback, H.R., UCLA, HHMI
Cross, T.A., NHMFL/FSU, Chemistry and Molecular Biophysics

Solid state NMR is now emerging as an important technique to study structures of integral membrane proteins. Dipolar couplings between selectively labeled groups can be measured to determine distance constraints in oriented protein and peptide samples. We developed a combination of genetic engineering and specific ^{19}F chemical labeling as an alternative NMR method to probe the structure of a 42 kD membrane protein, lactose permease of *E. coli*. Double-cys mutants were constructed in functional lac permease devoid of native Cys residues. Proteins were purified, labeled with thiol specific reagent p-fluorobenzene- thiol (FBT) and reconstituted into *E coli* membranes. Oriented samples were prepared from reconstituted proteoliposomes. ^{31}P NMR was used to examine the orientation of the *E. coli* lipids that surround the lac permease.[3]

As shown in Fig. 1, two ^{31}P NMR peaks were observed. The peak at 20 ppm represented the anisotropic chemical shift of the oriented lipid components. The unoriented lipids gave a powder pattern peak at -15 ppm. The ratio between these two peaks indicated that more than 90% of the protein was oriented. Fig. 2 shows the ^{19}F NMR spectra obtained from 300 MHz NMR spectrometer of oriented 302C/325C and 302C (as control) lactose permease mutans. The dash lines represent the experimental spectrum, while the solid line shows the simulated spectrum with a dipolar coupling of 2.3 kHz and the anisotropic chemical shift difference of 4.1 kHz. ^{19}F labels should be very similar. However, a slightly different orientation with respect to B_0 could easily result in such an anisotropy chemical shift difference. Assuming that the FBT probes are perpendicular to the protein helix so that the internuclear vector between the two ^{19}F labels is perpendicular to the B_0, the ^{19}F-^{19}F dipolar coupling of 2.3 kHz observed indicates that the distance between the two probes is 3.6 Å.

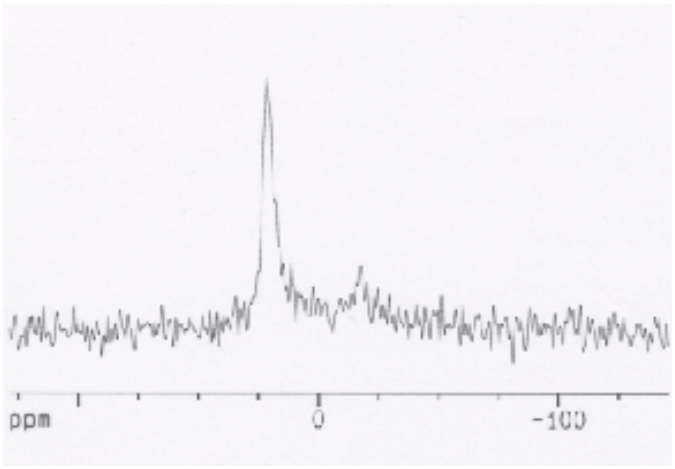

Figure 1. ^{31}P NMR Spectrum of oriented sample of the 302C/325C mutant labeled with FBT.

This result gives direct evidence that residues at position 302 and 325 are in close proximity, which agrees well with the previous conclusions.[1,2] A CPMG spectrum[4] should clearly indicate such a dipolar splitting. Samples are currently being tested on the 830 MHz solid state NMR for such an experiment.

It is clear that in using this approach, many intramolecular distance constraints can be obtained to assemble a well-defined three-dimensional helical packing structure of the lactose permease. Thus, ^{19}F solid state NMR, a highly sensitive method, can be used to provide insight into the structure of hydrophobic membrane proteins.

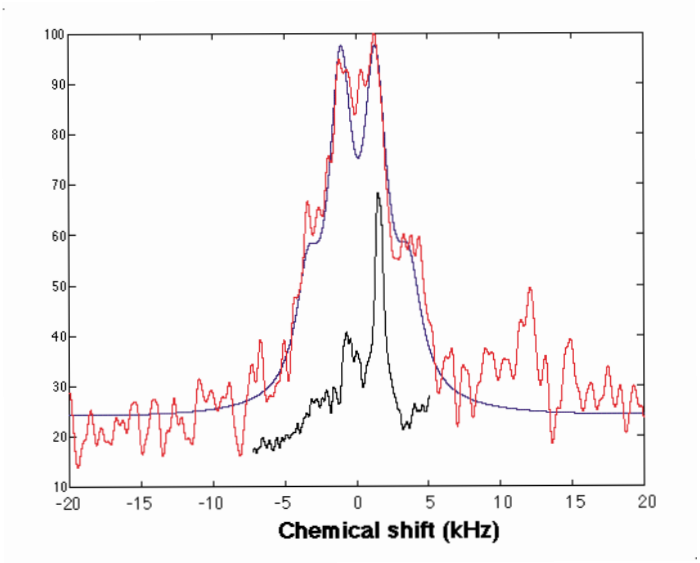

Figure 2. ^{19F}NMR spectra of oriented lactose permease in E. coli lipids. The dash lines represent the experimental spectra of 302C/325C and 302C (at low scale), while the solid line shows the simulated spectrum with a dipolar coupling of 2.3 kHz and the anisotropic chemical shift difference of 4.1 kHz. The heavy line represents the experimental spectrum of 302C.

[1] Kaback, H.R., *et al.,* Acc. Chem Res., **32**, 800-813 (1999).
[2] Frillingos, S., *et al.,* The FASEB Journal, **12**, 1281-1299 (1998).
[3] Cross, T.A., Annual Report on NMR Spectroscopy, **29**, 123-167 (1994).
[4] Grage, S.L., *et al.,* J. Magn. Reson., **138**, 98-106 (1999).

Effect of High Magnetic Field on Mammalian Cancer Cells

Haik, Y., FAMU-FSU College of Engineering
Chen, C., FAMU-FSU CoE
Badisa, R., Walker Cancer Institute

The recent advancement in producing high fields, together with an interest in enhancing the radiation dose delivered to small tumors with radioimmunotherapy, have triggered research to understand the cellular effects of prolonged exposure

to high fields. Researchers studied the effect of high magnetic fields on three malignant human cell lines HTB 63 (melanoma), HTB 77IP3 (ovarian carcinoma), and CCL 86 (lymphoma: Raji cells) which were exposed to a 7 T steady magnetic field for 64 hrs. The exposure to the magnetic field was found to produce a reduction in viable cell number in each of the three cell lines by an average of 26%.

Magnetic fields have been shown to alter gene expression. Expression of genes such as heat shock protein-70 (HSP70) and *c*-fos is induced when exposed to magnetic fields as low as 8 mT for 20 min. This is significant not only because these fields are so low, but also because these genes play roles in many important processes including cell division, cell death, and cellular repair following damage.

Recently, we have investigated the effects of high magnetic fields on leukemia, CaCoII, and HEP G2 cell lines. We found that when leukemia cells are exposed to a 12 T field for 2 hours there is an increase in cell death by about 30% compared to cells that were not exposed to the magnetic field. Fig. 1 shows the percentage of cell death for leukemia cells that were exposed for 1 hr and 2 hrs to a 12 T magnet compared to the control. The percentage of cell death was measured on three consecutive days after the exposure. Viability of CaCoII cells sandwiched between permanent magnets of maximum strength of 1.2 T was measured. A decrease in viable cells by 33% was found for exposed cells compared to unexposed cells. Our results together with other investigators' reports suggest a strong evidence of a reduction in the cell growth rate for cancer cells when subjected to high magnetic field.

One of the advantages to invoke strong magnetic field therapy compared to existing treatment methods and therapies is that magnetic fields can act non–invasively. Several experiments are currently planned to further study these phenomena.

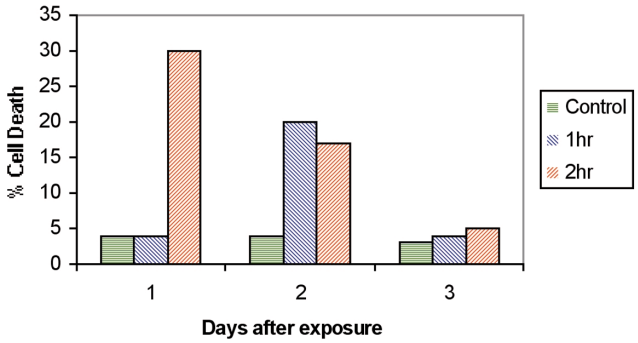

Figure 1. Percent of cell death measured in 3 days after exposure.

Baseline Mass Resolution of Peptide Isobars: A New Record for Molecular Mass Resolution

He, F., NHMFL
Hendrickson, C.L., NHMFL
Marshall, A.G., NHMFL/FSU, Chemistry

Baseline resolution of two peptides, RVMRGMR and RSHRGHR, of neutral monoisotopic mass, ~904 Da, has been achieved by microelectrospray ionization Fourier transform ion cyclotron resonance (FT-ICR) mass spectrometry at a mass resolving power of ~3,300,000. The elemental compositions of these molecules differ by N_4O vs. S_2H_8 (0.00045 Da), which is less than one electron's mass (0.00055 Da)! This result establishes a new record for the smallest resolved mass difference between any two molecules. This achievement is made possible by a combination of high magnetic field (9.4 T), large diameter (4-inch) Penning trap, and low ion density. The implications for proteomics based on accurate mass measurements are discussed briefly in Ref. 1.

Acknowledgements: This work was supported by grants from the NSF National High Field FT-ICR Mass Spectrometry Facility (CHE-99-09502), NIH (GM-31683), FSU, and the NHMFL.

[1] He, F., *et al*., "Baseline Mass Resolution of Peptide Isobars: A New Record for Molecular Mass Resolution," Anal. Chem., **73**, 0000-0000 (2001).

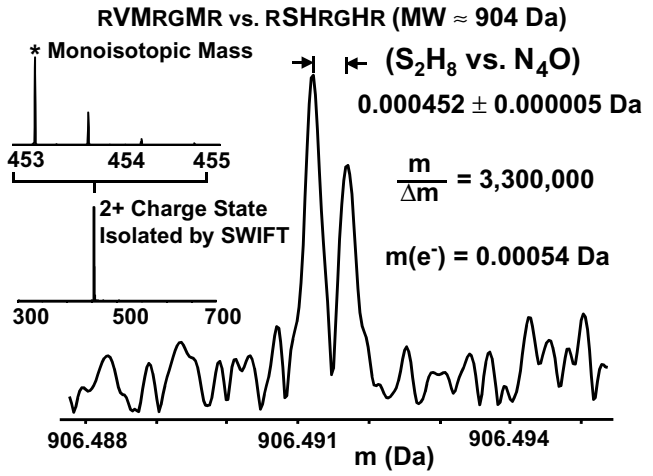

Figure 1. Ultrahigh-resolution electrospray 9.4 T FT-ICR mass spectrum of two equimolar peptides, RVMRGMR and RSHRGHR, detected in digital quadrature heterodyne (narrowband) mode. The doubly-charged ions were isolated by stored-waveform inverse Fourier transform (SWIFT) dipolar ejection. The two peptides differing in mass by 0.00045 Da are baseline-resolved. The achieved resolving power is $m/\Delta m_{50\%}$ = 3,300,000, in which $\Delta m_{50\%}$ is the magnitude-mode peak full width at half-maximum peak height.

Unequivocal Determination of Metal Atom Oxidation State in Naked Heme Proteins: Fe(III)Myoglobin, Fe(III)Cytochrome *c*, Fe(III)Cytochrome b5, and Fe(III)Cytochrome b5 L47R

He, F., NHMFL
Hendrickson, C.L., NHMFL
Marshall, A.G., NHMFL/FSU, Chemistry

Unambiguous determination of metal atom oxidation state in an intact metalloprotein is achieved by matching experimental (electrospray ionization 9.4 T Fourier transform ion cyclotron resonance) and theoretical isotopic abundance mass distributions for one or more holoprotein charge states. The iron atom oxidation state is determined unequivocally as Fe(III) for each of four gas-phase unhydrated heme proteins electrosprayed from H_2O: myoglobin, cytochrome *c*, cytochrome b5, and cytochrome b5 L47R (i.e., the solution-phase oxidation state is conserved following electrospray to produce gas-phase ions). However, the same Fe(III) oxidation state in all four heme proteins is observed after prior reduction by sodium dithionite to produce Fe(II) heme proteins in solution: thus proving that oxygen was present during the electrospray process. Those results bear directly on the issue of similarity (or lack thereof) of solution-phase and gas-phase protein conformations. Finally, infrared multiphoton irradiation of the gas-phase Fe(III)holoproteins releases Fe(III)heme from each of the non-covalently bound Fe(III)heme proteins (myoglobin, cytochrome b5 and cytochrome b5 L47R), but yields Fe(II)heme from the covalently bound heme in cytochrome *c*.

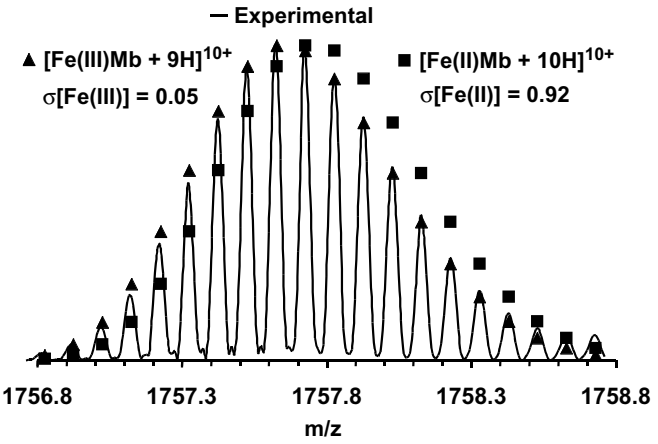

Figure 1. Experimental ESI FT-ICR mass spectral segment of horse skeletal holomyoglobin, showing the 10+ charge state. The solid line is experimental data whereas the squares and triangles are the theoretical isotopic relative abundances for $[Fe(II) + 10H]^{10+}$ and $[Fe(III) + 9H]^{10+}$. The lower standard deviation between experimental and theoretical isotopic relative abundances establishes Fe(III) as the correct oxidation state.

Acknowledgements: The authors thank Dr. Mark R. Emmett and Dr. Weiqun Li for helpful discussions. We also thank Dr. Marshall Pope for kindly providing samples of Cyt b5 and its L47R mutant. This work was supported by grants from the NSF National High Field FT-ICR Mass Spectrometry Facility (CHE-94-13008), NIH(GM-31683), FSU, and the NHMFL.

[1] He, F., *et al*., J. Am. Soc. Mass Spectrom., **11**, 120-126 (2000).

Behavioral and Neural Effects of Static High Magnetic Fields

Houpt, T.A., FSU, Biological Science
Smith, J.C., FSU, Psychology
Jahng, J.W., Yonsei College of Medicine, Pharmacology, Korea
Pittman, D., FSU, Neuroscience
Barranco, J.M., FSU, Biological Science

Advances in magnetic resonance imaging (MRI) are driving the development of faster and higher resolution MRI machines. Little is known about the sensory or physiological effects of static magnetic fields of high strength on mammals and humans. We have recently discovered that 30 min. exposure to a 9.4 T magnetic field has behavioral and neural effects on a rat. At the behavioral level, magnetic field exposure induced a conditioned taste aversion (CTA) after pairing with the taste of saccharin. Because CTA has proven to be a sensitive index of visceral malaise, this suggests that the magnetic field may be an aversive stimulus to the rat. At the neural level, the same exposure induced specific and significant c-Fos immunoreactivity, a marker of neuronal activation, in the rat brainstem, especially in visceral and vestibular brain regions.

In the past year, we have extended this observation by exposing rats to superconducting magnets of 7 T, 9.4 T, and 14 T, and to a resistive magnet at 14 T. We have found graded effects on taste aversion and c-Fos, such that 7 T is barely capable of inducing taste aversion or c-Fos, while 14 T is more potent at both the behavioral and neural levels. We have also begun to quantify the behavioral effects of the magnet fields by videotaping the rats in a large test chamber when they are removed from the magnet. For example, magnet-exposed rats were confined in a Plexiglas tube and positioned vertically (heads-up) for 30 min. within the 14 T magnet. Sham-exposed rats were restricted in the same manner for the 30-min. period, but not exposed to the magnetic field. When the rats were released from the magnet, the majority walked in tight circles as if suffering an inner ear or balance problem. None of the sham-exposed rats displayed this circling behavior. Furthermore, all of the rats exposed to the magnetic field with their heads-up circled *counter-clockwise.* Intriguingly, rats confined within the 14 T magnet in the heads-down position also circled upon release, but they circled *clockwise* (see Fig. 1). Both the behavioral response and the pattern of c-Fos activation are similar to the effects of vestibular disturbance, such as rotation and motion sickness. Therefore, our working hypothesis is that the magnetic field activates the vestibular apparatus of the inner ear, causing vertigo and CTA acquisition.

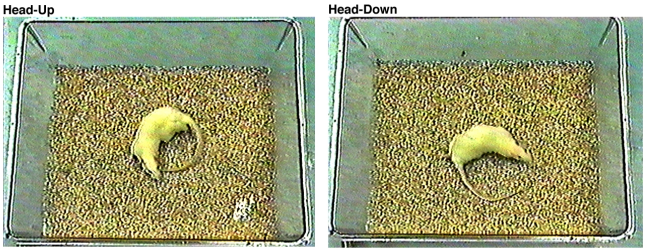

Figure 1. Still video frames of rats displaying tight circling behavior after 30 min. oriented heads-up (left) or heads-down (right) within a 14 T field.

A 330 GHz EPR Study of the Semiquinone Biradical $Q_A^{-\bullet}Q_B^{-\bullet}$ in Photosynthetic Reaction Centers of *Rb. Sphaeroides*

Isaacson, R.A., Univ. of California, San Diego, Physics
Calvo, R., FBCB & INTEC, Argentina
Abresch, E.C., UCSD, Physics
Paddock, M.L., UCSD, Physics
Maniero, A., Univ. of Padova, Physical Chemistry
Saylor, C., NHMFL
Brunel, L., NHMFL
Feher, G., UCSD, Physics

One of the important intermediate states in the primary processes of bacterial photosynthesis is formed by the semiquinone biradical $Q_A^{-\bullet}Q_B^{-\bullet}$. We have previously studied the spatial and electronic structure of $Q_A^{-\bullet}Q_B^{-\bullet}$ by EPR at 9, 35 and 94 GHz.[1] Of particular importance for understanding electron transfer is the exchange interaction, J_o, defined by $H_{exch} = -J_o \mathbf{S_A}\bullet\mathbf{S_B}$. Unfortunately, the EPR spectra are

relatively insensitive to J_o at frequencies up to ~100 GHz. Consequently, the accuracy of J_o that we obtained[1] was rather poor (J_o= −60±20 MHz). However, at 330 GHz,[2] transitions that were not easily observed at 94 GHz become prominent. Fig. 1 shows a comparison between spectra taken at 94 GHz and 326 GHz. The vertical arrows indicate lines that show up only at the higher frequencies. Their positions, which are temperature dependent, enabled us to determine J_o with a higher accuracy. Data was taken at temperatures from 5 K to 120 K and global fitting was done using the simulated annealing method.[3] A new value of J_o (−82±3 MHz) was obtained, with much better accuracy than the previous value quoted above. The more accurate value of $J_{o,}$ obtained from the data at 326 GHz, allows us to estimate with greater confidence a maximum electron transfer rate between the semiquinones. [1]

$$k_{ET}^{max} \approx 10^{9-1}$$

Considering the distance 17 Å, between $Q_A^{-\bullet}$ and $Q_B^{-\bullet}$, this value is larger than expected, from a compilation of values in other proteins, suggesting that in RCs the intervening media is a better conductor than the average protein.

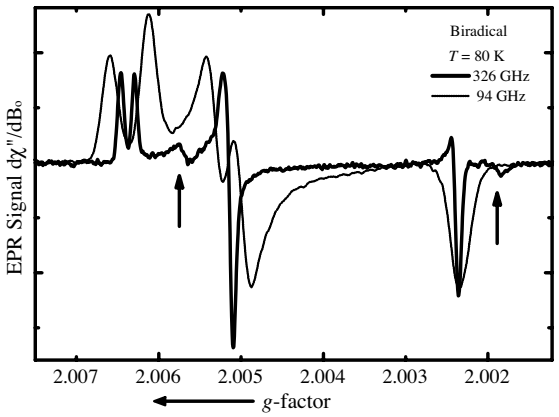

Figure 1. EPR spectra of the $Q_A^{-\bullet}Q_B^{-\bullet}$ biradical in reaction centers from *Rb. Sphaeroides* at 94 and 326 GHz. The signal is plotted using the g-value rather than magnetic field for a more direct comparison.

Acknowledgments: This work was supported by grants of NIH (GM 41637, GM 13191) and NSF (MCB 94-16652).

[1] Calvo, R., *et al*., J. Am. Chem. Soc., **122**, 7327-7341 (2000).
[2] Hassan, A.K., *et al.,* Appl. Magn. Reson., **16**, 299-308 (1999).
[3] Kirkpatrick, S., *et al*., Science, **220**, 671-680 (1983).

Domain Dynamics of Smooth Muscle Myosin

Li, H., NHMFL/FSU
Fajer, P.G., NHMFL/FSU, Biology and Institute of Molecular Biophysics

The myosin head (subfragment 1, S1) plays a central role during muscle contraction. It is thought that during the ATPase cycle, the catalytic domain of S1 interacts with actin and a rotation of the regulatory domain with respect to the catalytic domain resulting in a directional strain on the actin filaments. The structure of the myosin head shows two distinct domains: a motor domain with catalytic and actin binding properties, and an extended neck region ("regulatory domain") that consists of the essential and regulatory light chains and the α-helical heavy chain to which they bind.

In this study, we hypothesize that the domain dynamics in a myosin head is closely related to its function. We characterized the regulatory and catalytic domain dynamics of the smooth muscle myosin in solution, filaments, and in actomyosin complex. Consistent with the skeletal muscle myosin, the regulatory and catalytic domains of a myosin head have independent mobility (Fig. 1), supporting the idea that a hinge exists between the two domains. When the domain dynamics is compared between the smooth and skeletal muscle myosin, the smooth muscle myosin regulatory domain has a much more restricted freedom of motion, and this motional constraint is dictated by the myosin heavy chain (Fig. 2).

Figure 1. ST-EPR spectra of catalytic (Cys717) and regulatory domains (Cys108 of RLC) of smooth muscle myosin.

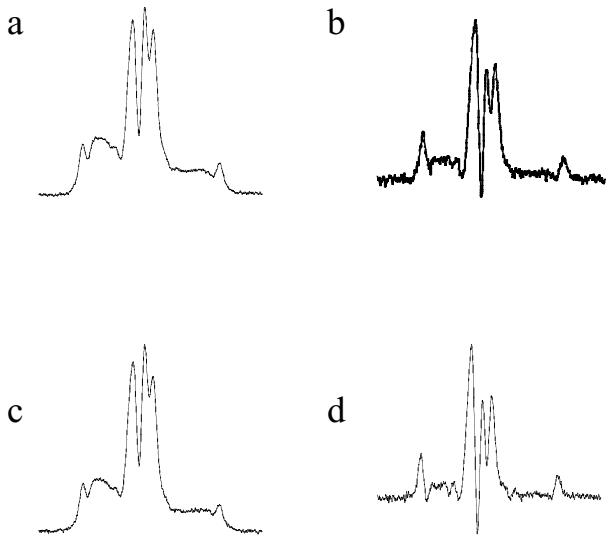

Figure 2. ST-EPR spectra of regulatory domain from different myosin isoforms. (a) Smooth HC exchanged with smooth RLC, (b) skeletal HC exchanged with skeletal RLC, (c) smooth HC exchanged with skeletal RLC, and (d) skeletal HC exchanged with smooth RLC. The mobility of the "hybrids" (c, d) were compared with the "native" ones (a, b).

Influence of Transmembrane Peptides on Bilayers of Phosphatidylcholines with Different Acyl Chain Lengths Studied by Solid State NMR

Lindblom, G., Umeå Univ., Chemistry and Biophysical Chemistry
Byström, T., Umeå Univ., Chemistry and Biophysical Chemistry
Strandberg, E., Umeå Univ., Chemistry and Biophysical Chemistry
Kovacs, F.A., NHMFL/FSU, Molecular Biophysics
Cross, T.A., NHMFL/FSU, Chemistry

The molecular orientation in a lipid membrane of the peptide fragment, VEYAGIALFFVAAVLTLWSML-QYLSAAR (phosphatidylglycerophosphate synthase (Pgs) peptide E), of an integral membrane protein, Pgs, in Escherichia coli has been investigated by solid-state ^{15}N NMR on macroscopically aligned lipid bilayers (Fig. 1). The secondary structure of the peptide in lipid vesicles was determined by circular dichroism spectroscopy. Furthermore, the phase behavior of the Pgs peptide E/dierucoylphosphatidylcholine (DeruPC)/water system was determined by ^{2}H, ^{31}P and ^{15}N solid-state NMR spectroscopy. The phase behavior obtained was then compared to that of the Pgs peptide E solubilized in dioleoylphosphaidylcholine and water that was previously studied by Morein *et al.*[1] This was aimed to answer the question of whether a difference in the length of the hydrophobic part of this peptide and the hydrophobic thickness of the lipid bilayer (hydrophobic mismatch) would affect the phase behavior.

The peptide mostly has a transmembrane orientation and is in an alpha helical conformation. An isotropic phase is formed in DeruPC with high peptide content (peptide/lipid molar ratio≥1:15) and high water content (≥50% w/w) at 35°C. At 55 and 65°C, an isotropic phase is induced at high water content (≥50% w/w) at all peptide contents studied (no isotropic phase forms in the lipid/water system under the conditions in this study). At high peptide contents (≥ 1:15), an isotropic phase forms at 20 and 40% water at 55 and 65°C. A comparison of the phase

behavior of the two homologous lipid systems reveals striking similarities, although the thickness of the two lipid bilayers differ by 7Å. This suggests that the rationalization of the phase behavior in terms of the hydrophobic mismatch is not applicable to these systems. The C-terminus of Pgs peptide E is amphiphilic and a considerable part of the peptide is situated outside the hydrophobic part of the bilayer, a property of the peptide that to a large extent will affect the lipid/peptide phase behavior.[2]

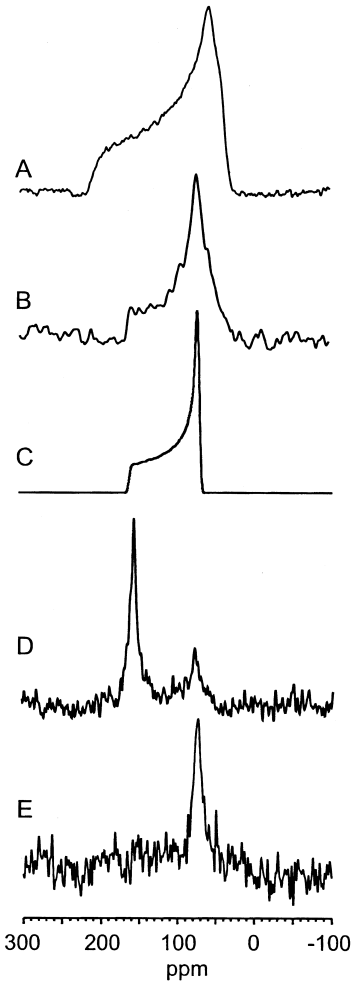

Figure 1. ^{15}N NMR spectra of Pgs peptide E samples. (A) Spectrum of dry powder sample. (B) Spectrum at 39°C of a hydrated sample in DOPC/water–1:7 molar ratio and 20% water. (C) Simulated spectrum of B. (D) Spectrum of aligned sample (bilayer normal parallel to applied magnetic field) with a molar ratio of 1:16 and 50% water. (E) As in D, but with the sample alignment axis perpendicular to the applied magnetic field.

[1] Morein, S., *et al.,* Biophys. J., **73,** 3078-3088 (1997).

[2] Bystrom, *et al.,* Biochim. Biophys. Acta, **1509,** 335-345 (2000).

Analysis of Transdermal Drug Delivery: The Effects of Model Penetration Enhancers on Skin Transport Properties

Locke, B.R., FAMU-FSU College of Engineering
Gibbs, S.J., FAMU-FSU College of Engineering
Moerland, T.S., FSU, Biological Science
Caban, J.B., FSU, Molecular Biophysics

Transdermal drug delivery offers advantages over conventional oral or hypodermic delivery of drugs. However, only a small number of compounds are sufficiently permeable to cross the skin at rates adequate to be clinically useful. Previous work has shown that chemical penetration enhancers are able to increase the permeability of skin and increase the range of compounds that can be delivered transdermally. In this project, diffusion weighted magnetic resonance microscopy (μMRI) was used to analyze the transport of solutes through the skin of hairless rats (which resembles human skin), after treatment with model penetration enhancers, including urea, ethanol, DMSO, and SDS. These compounds are thought to temporarily alter the structural organization or chemical composition of the skin, thus allowing increased rates of transport. Chemical modification of the skin may enhance the ability of compounds to cross the skin via "shunt" pathways, such as hair follicles. Magnetic resonance microscopy can provide both structural information and transport coefficients, and is a technique that is well suited for determining the importance of shunt pathways in transdermal transport.

Work in the past year has focused on the effects of the exposure time of penetration enhancers on skin transport properties. Data were acquired with the wide-bore 600 MHz Bruker DMX spectrometer system at the NHMFL. In-plane resolution of 39x39x200 μm permitted visualization of the components of skin thought to play a significant role in transdermal drug delivery, the viable epidermis, hair follicle, and stratum corneum regions. Two significant results are apparent (Tab. 1): The apparent water self-diffusion coefficient increases with increasing exposure time for all penetration enhancers examined. Moreover, the DMSO data show that the water

diffusion coefficient is higher in the viable epidermis than in the hair follicle region, a result apparent only with this penetration enhancer. Further investigation will examine the effects of penetration enhancers and electric fields applied simultaneously in order to determine if their combined application yields even high skin permeability.

Acknowledgements: This work was supported in part by a grant from the Whitaker Foundation.

Table 1.

		Diffusion Coefficient ± SE (cm^2s^{-1})		
		4.5 h Exposure	9.0 h Exposure	13.5 h Exposure
100% H_2O	Epidermis	$6.66\times10^{-6}\pm 1.31\times10^{-7}$	$6.66\times10^{-6}\pm 1.32\times10^{-7}$	$6.66\times10^{-6}\pm 1.32\times10^{-7}$
	Hair	$7.39\times10^{-6}\pm$	$7.40\times10^{-6}\pm$	$7.38\times10^{-6}\pm$
	Follicle	1.27×10^{-7}	1.27×10^{-7}	1.27×10^{-7}
10% Urea	Epidermis	$8.93\times10^{-6}\pm 5.56\times10^{-7}$	$1.15\times10^{-5}\pm 1.04\times10^{-6}$	$1.71\times10^{-5}\pm 1.60\times10^{-6}$
	Hair	$9.71\times10^{-6}\pm$	$1.40\times10^{-5}\pm$	$1.92\times10^{-5}\pm$
	Follicle	6.70×10^{-7}	8.49×10^{-7}	1.11×10^{-6}
100% EtOH	Epidermis	$8.48\times10^{-6}\pm 2.94\times10^{-7}$	$1.10\times10^{-5}\pm 6.05\times10^{-7}$	$1.38\times10^{-5}\pm 8.31\times10^{-7}$
	Hair	$1.00\times10^{-5}\pm$	$1.34\times10^{-5}\pm$	$1.72\times10^{-5}\pm$
	Follicle	4.35×10^{-7}	7.57×10^{-7}	7.94×10^{-7}
100% DMSO	Epidermis	$9.33\times10^{-6}\pm 2.71\times10^{-7}$	$1.07\times10^{-5}\pm 6.36\times10^{-7}$	$1.18\times10^{-5}\pm 8.98\times10^{-7}$
	Hair	$8.88\times10^{-6}\pm$	$9.21\times10^{-6}\pm$	$9.66\times10^{-6}\pm$
	Follicle	2.53×10^{-7}	2.77×10^{-7}	3.00×10^{-7}
20% DMSO	Epidermis	$9.17\times10^{-6}\pm 5.04\times10^{-7}$	$9.73\times10^{-6}\pm 1.91\times10^{-7}$	$1.15\times10^{-5}\pm 5.20\times10^{-7}$
	Hair	$8.29\times10^{-6}\pm$	$9.18\times10^{-6}\pm$	$9.43\times10^{-6}\pm$
	Follicle	2.09×10^{-7}	5.89×10^{-8}	2.21×10^{-7}
10% SDS	Epidermis	$1.12\times10^{-5}\pm 6.09\times10^{-7}$	$1.24\times10^{-5}\pm 6.81\times10^{-7}$	$1.51\times10^{-5}\pm 8.91\times10^{-7}$
	Hair	$1.23\times10^{-5}\pm$	$1.37\times10^{-5}\pm$	$1.65\times10^{-5}\pm$
	Follicle	7.03×10^{-7}	7.52×10^{-7}	6.84×10^{-7}

Electrochemical Cancer Therapy Analysis by MRI

Locke, B.R., FAMU-FSU College of Engineering, Chemical Engineering
Moerland, T.S., FSU, Biological Sciences
Gibbs, S.J., NHMFL/FAMU-FSU CoE-CE
Caban, J., FSU, Institute of Molecular Biology
Dev, S.B., Genetronics, Inc.

Recently, a new modality of cancer treatment has been introduced which combines pulsed electric fields (PEF) with anticancer drugs. PEF create transient pores in the cell membrane allowing the entry of drugs into the cells. This method increases cytotoxicity of some anticancer drugs like bleomycin (BLM) by 2 to 3 orders of magnitude, which in turn, reduces systemic drug dosage without decreasing efficacy.

In this study, magnetic resonance imaging (MRI) was used to study the structural changes that occur in an animal laryngeal tumor (HEp-2 cells) model with BLM delivered by PEF. The instrument used was a Bruker wide-bore 600 MHz spectrometer equipped with micro-imaging capability. Mice carrying ~8 mm (maximum dimension) tumors were treated with several combinations of drug and PEF. Standard MRI protocols were used to determine the spatial dependence of the spin-lattice relaxation time (T_1), the spin-spin relaxation time (T_2), and the apparent water intra-diffusion coefficient (ADC). All three measurements were made on tumor samples excised from mice 24 and 48 hours after treatment with (i) saline, (ii) BLM, (iii) saline with PEF, or (iv) BLM injection, followed by PEF.

Although T_1 does not differ between the controls (i, ii, and iii) and full treatment (iv) [6.72+/-0.20 s vs. 6.31 +/- 1.7 s], T_2 for (iv) at 24 hours is significantly different from the controls [52.4 +/-0.91 ms vs.46.5 +/- 1.54 ms]. This difference disappears at 48 hours. ADC increases significantly from 24 to 48 hours [$7.31+/-0.16\times10^{-6}$ to $8.28+/-0.28\times10^{-6}$ cm^2/sec, $p=0.05$, $n=8$]. Longer T_2 values may reflect early apoptosis and tumor death when the tumor is structurally less dense. Higher ADC's, associated with the periphery of the tumors and the central region, may indicate loose structural organization and necrosis resulting from combination treatment.

Initial Steps in the Folding of the FK506 Binding Protein

Logan, T.M., FSU, Chemistry
Korepanova, A., FSU, Molecular Biophysics
Palmer, A., FSU, Chemistry

We are investigating how non-random conformational averaging in unfolded proteins affects or effects subsequent folding. The main objective is to obtain a more thorough understanding of how protein folding begins. Our approach is to create site-mutants in our protein, the FK506 binding protein (FKBP), and measure thermodynamic stability and kinetic properties of the mutant. As an essential part of our research project, we use multidimensional NMR

spectroscopy to characterize the structure of the native and unfolded states of FKBP mutants. We want to determine, first, if there are any changes in mutant protein structures compared to the wild type under native conditions, and, second, to characterize potential changes in the elements of residual structure earlier shown for urea unfolded FKBP. All NMR experiments were run at 30 °C on 500 MHz and 600 MHz spectrometers equipped with a triple resonance (H, N, C) probes.

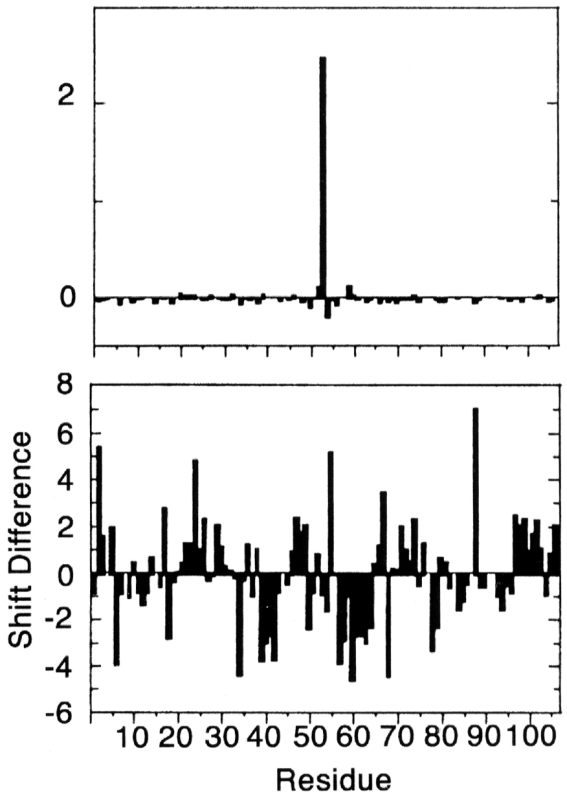

Figure 1. Cα chemical shift index values for gsFKBP (bottom). Groupings of positive values indicate β-sheet formation, groupings of negative values indicate α-helix. Cα shift difference between gsFKBP and Q53N mutant (top). Note change in scale. The shift differences between the two FKBP variants is minimal even compared to the shift differences within a single protein.

We have run complete sets of triple resonance experiments to assign backbone ^{1}H, ^{15}N, and ^{13}C resonances of our wildtype and all mutant proteins in the native state. Additional structural information is obtained from an analysis of $^{3}J_{HNHA}$ scalar coupling constants and medium- and long-range NOE patterns in 3D ^{15}N-separated NOESY-HSQC spectra.

We observe that mutations to position Q53 have little effect on the native state structure, in general. Slight changes in backbone chemical shifts are observed for residues that are immediately adjacent to the mutation site in the primary sequence (Fig. 1), but little change is observed for residues that are adjacent to the mutation site in the three dimensional structure. Q53 is a surface-exposed residue in a region of non-regular secondary structure in native FKBP. Interestingly, mutations to this residue have effects on thermodynamic stability and kinetic folding that are best explained by changes in the conformational averaging of the unfolded state and structural changes that occur during folding. We are currently using multidimensional NMR to investigate conformational averaging in the unfolded state of FKBP and its mutants.

Unique Ligands of the Leucine Binding Proteins: A ^{19}F NMR Study

Luck, L., Clarkson Univ., Chemistry
Sondi, B., Clarkson Univ., Chemistry
Johnson, B., Clarkson Univ., Chemistry

Periplasmic binding proteins serve as initial receptors of active transport for a wide variety of substrates. Two proteins which bind hydrophobic-branched amino acids, leucine/isoleucine/valine-binding protein (LIV) and the leucine specific binding protein (LS) share the same overall structure but have different specificities. LS was thought to bind only leucine and trifluoroleucine where LIV binds leucine, isoleucine, threonine, and valine. Selectivity for the ligand is achieved by a cleft lined with hydrophobic residues. One of the most obvious differences between these two proteins is position 18, where LS has a Trp residue and LIV has a Tyr. To address this critical variance and further understand the method of binding differentiation, mutant LIV(YW18) and LS(WY18) were made along with site directed mutants for all of the Trp residues.

Our work has demonstrated that LS and LIV(YW18) have a much wider range of substrates including Phe and fluorinated analogues of Phe. We have

biosynthetically incorporated 5F-Trp into these proteins. NMR studies have shown that Trp18 is involved in binding of the substrates and experiences two distinct environments in the binding pocket. We also have observed a large hinge-bending motion that shows two dissimilar conformations when Leu and Phe bind to the cleft. ^{19}F NMR studies show that LS(W320F) and LS(W336F) show more flexible conformations without leucine in the binding pocket. The Trp residues near the hinge are key to holding the structure in a defined conformation in the open form. Our studies have shown that the hydrophobic receptors may be more open and flexible than the other periplasmic binding proteins and very similar to the steroid hormone receptors.

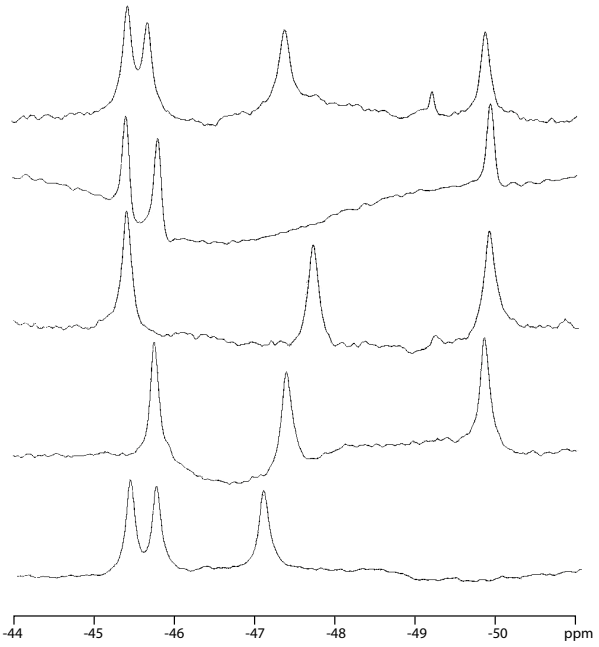

Figure 1. The 470 MHz ^{19}F NMR spectra of the wild type and site directed mutants unequivocally assigning the resonances to the Trp residues in the LS protein. Spectra were obtained in less than 15 minutes with a 1 second recycling delay. 100% incorporation of 5F-Trp was calculated for each protein.

Comparison of Gramicidin A and Gramicidin M Channel Conductance Dispersion Properties

Markham, J.C., Brigham Young Univ., Zoology and Neuroscience
Merrell, J.D., Brigham Young Univ., Zoology and Neuroscience
Cross, T.A., NHMFL/FSU, Chemistry and Molecular Biophysics
Busath, D.D., Brigham Young Univ., Zoology and Neuroscience

Understanding the relationship between amino acid sequence and biological function is a long standing goal in biology. At the NHMFL, the relatively small protein, known as gramicidin, has been structurally characterized to higher resolution than any other membrane protein. In addition, at Brigham Young University the function of this cation channel is being characterized in exquisite detail. Consequently, there is a unique opportunity through studies of gramicidin to learn more about this important relationship between sequence and function.

Gramicidin A (gA) has one principle channel conductance rate, referred to herein as the standard conductance, with a broad range of substate conductances referred to as "minis." These mini channel variants have been thought to be caused at least in part by the tryptophan side chains. Experiments were performed with gramicidin M (gM), a gramicidin variant in which all four tryptophan residues are replaced with phenylalanine residues, and its enantiomer, gramicidin M- (gM-). The conductance of highly purified gM and gM- was studied in KCl, NaCl, and HCl at a variety of concentrations, voltages, and in two different types of lipid.

These experiments showed that the channels with conductances in the range of 50 to 90% of the standard are absent in gM. On the other hand, gM and gM- were observed to have a prominent population of minis in a sharp peak which have conductances less than 50% of the standard type. We conclude that the mini channels not found in gM are caused in gA by

some structural aberration related to the tryptophan side chains. In other words, a conformational substate of the side chain conformation could cause this significant change in the conductance state. In addition, some other variation in configuration not related to tryptophan side chains causes low conductance minis in gM and gM-. These minis have reduced channel lifetimes, but unchanged current-voltage curvature compared to standards, suggesting increased strain in the dimer, but without a significant increase in the barrier to ion passage.

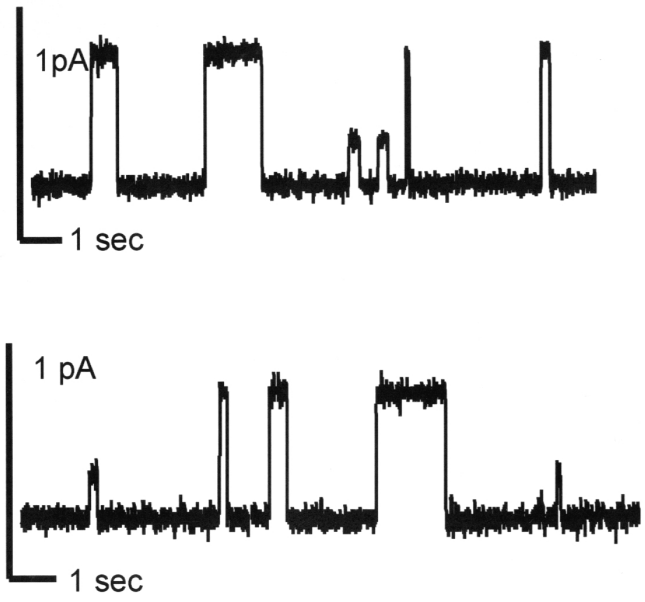

Figure 1. Representative traces of gramicidin M channel conductance in 1 M KCl with a 100 mV potential across the membranes formed from glycerol mono-olein (GMO).

Structural Studies of Gramicidin A in Long-Chain Lipid Bilayers by Solid State NMR

Mo, Y., NHMFL/FSU, Chemistry
Tian, C., NHMFL/FSU, Molecular Biophysics
Cross, T.A., NHMFL/FSU, Chemistry and Molecular Biophysics

Gramicidin A (gA) is a 15 amino acid polypeptide from *Bacillus brevis*. As a dimer, it forms a monovalent cation selective channel across lipid bilayers. The channel, due to its alternating pattern of D and L stereochemistry, has a $\beta^{6.5}$ helical structure. The conducting state is a single stranded dimer spanning the lipid bilayer. Single channel conductance clearly shows that gating of this channel results from the monomer-dimer equilibrium. The structure of the open state of gA has been well resolved by solid state NMR, yet no structural evidence for the (presumably monomeric) closed state has been obtained. In the long chain lipids bilayers, the hydrophobic mismatch between the bilayer and gA results in a shift of the monomer-dimer equilibrium towards the monomeric state. Here are some preliminary results.

Oriented samples of ^{15}N-(Ala-5)-labeled gA in Dierucoylphosphatidylcholine (22:1)(DEruPC) and Dinervonoylphosphatidylcholine (24:1) (DNPC) bilayers were prepared in this lab. The orientation of the bilayers was checked by ^{31}P spectroscopy. A substantial change was observed from the well-characterized dimeric state with a single sharp resonance at 198 ppm for this labeled site (Ala5 - Fig. 1). From ^{15}N solid state NMR spectra, the distribution of resonance frequencies suggests that there are many gA conformations in the long chain lipid bilayers. Potentially there are motions which further broaden the observed resonances.

Further experiments will be performed to optimize the sample for monomers structural characterization.

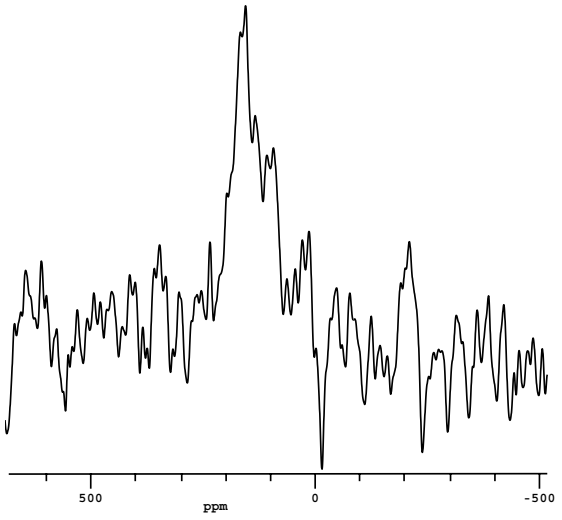

Figure 1. ^{15}N spectrum of ^{15}N-Ala$_5$-gA in DNPC bilayers. Peptide/Lipid molar ratio is 1:40.

Demembranization Reduces Diffusive Anisotropy of Creatine Phosphate in Skeletal Muscle

Moerland, T.S., FSU, Biological Sciences
Vanderlinde, O.H., FSU, Biological Sciences

Previous work has shown that diffusion of creatine phosphate, a metabolite important to energy metabolism, is highly anisotropic in muscle. Diffusion measured with the long axis of cylindrically shaped muscle fibers (longitudinally) is impeded less than diffusion measured across (radially). Diffusive anisotropy in muscle has been postulated to be a consequence of intracellular membrane barriers. Removal of these barriers, such as the sarcolema and mitochondrial membranes, allows for a direct test of this hypothesis by permitting measurement of their contribution to anisotropy.

Goldfish (*Carassius auratus*) red and white skeletal muscle was removed, and then demembranated in a glycerol solution containing Triton X-100 for 36 hours. Immediately following treatment, samples were fixed with a 20% paraformaldehyde, 25% glutaraldehyde fixative solution. After fixation, samples were bathed in a solution containing phosphorous metabolites that were lost during treatment. Diffusion of creatine phosphate (D_{PCr}) was determined by nuclear magnetic resonance (NMR) using a bipolar pulsed longitudinal eddy current delay sequence (BPP-LED). Measurements of diffusion were made over a time course of 15 to 300 ms. Diffusion measurements were also made in excised viable tissue in order to characterize the contribution of cellular barriers to diffusive anisotropy.

As shown in Fig. 1, analysis of radial and longitudinal D_{PCr} in both demembranated and viable tissue shows a significant decrease in anisotropy of demembranated tissue compared to viable tissue at long time points (>50 ms). The results indicate that removal of intracellular membranes also removes significant determinants of anisotropic diffusion.

Acknowledgements: The technical support of Lori McFadden is gratefully acknowledged. This research is supported by NSF IBN-98-08120.

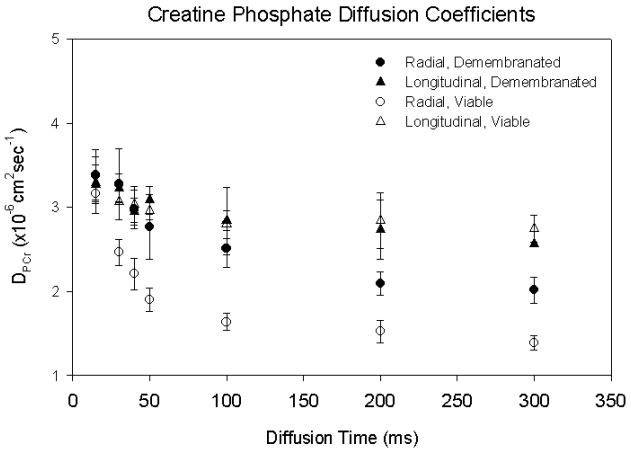

Figure 1. Diffusion coefficients of creatine phosphate in viable and demembranated preparations of goldfish oxidative (red) muscle. Removal of intracellular membranes markedly reduces diffusive anisotropy, indicating that these features are a principal barrier to diffusion within living cells.

High Magnetic Field Effects on Gene Expression in Transgenic Arabidopsis ◤IHRP◢

Morgan, A.N., UF, Physics and NHMFL
Yowtak, J., Univ. of Dallas, UF, Physics, and NHMFL
Meisel, M.W., NHMFL/UF, Physics
Brooks, J.S., NHMFL/FSU, Physics
Paul, A.-L., UF, Horticultural Sciences and Biotechnology
Ferl, R.J., UF, Horticultural Sciences and Biotechnology

We are using transgenic *Arabidopsis thaliana* (arabidopsis) as monitors of possible biological effects of high magnetic fields. The transgene is composed of an *alcohol dehydrogenese* (*Adh*) gene promoter that acts as the exogenous stress sensor and the gene for β-glucuronidase (GUS) as the reporter. The *Adh* promoter is sensitive to a variety of environmental stresses, making the *Adh*/GUS plants effective biomonitors for evaluating the impact of unique environments on a biological system at the

cellular level. The GUS activity can be evaluated qualitatively through histochemical staining, and quantitatively with spectrofluometric assays designed to detect the biochemical reaction of GUS in plant extracts with a known quantity of substrate. Arabidopsis plants were exposed to fields up to 25 T for a period of 2.5 hours. In preliminary data taken above 17 T, an increased GUS activity is found in both leaf and root tissue. Time courses from 0 to 3 hours at 20 T and from 0 to 48 hours at 9 T were performed in order to determine the importance of field exposure time. Additional work is necessary in order to clarify the trends represented in the preliminary data, and this work may have important implications for the potential use of high field NMR/MRI for biomedical, *in vivo* studies.

Acknowledgments: This work was supported, in part, by the NSF through the In-House Research Program of the NHMFL and the NHMFL REU Program (J.Y.).

Role of a Conserved Pseudouridine in Eukaryotic Branch Site RNA Structure

Newby, M.I., NHMFL/FSU, Molecular Biophysics
Greenbaum, N.L., NHMFL/FSU, Molecular Biophysics and Chemistry

The removal of non-coding sequences (introns) from eukaryotic precursor mRNA is catalyzed by the spliceosome, a dynamic assembly involving specific and sequential RNA-RNA and RNA-protein interactions. An essential RNA-RNA pairing between the U2 small nuclear (sn)RNA and a complementary consensus sequence of the intron, called the branch site, results in the positioning of the 2' OH of an unpaired adenosine residue to initiate nucleophilic attack in the first step of splicing (Fig. 1). In order to understand the structural features that facilitate recognition and chemical activity of the branch site from *Saccharomyces cerevisiae*, duplexes representing the paired U2 snRNA and intron sequences were examined by solution NMR spectroscopy. Oligomers were synthesized with pseudouridine(ψ) at a conserved site on the U2 snRNA strand (opposite an A-A dinucleotide on the intron strand) and with uridine,

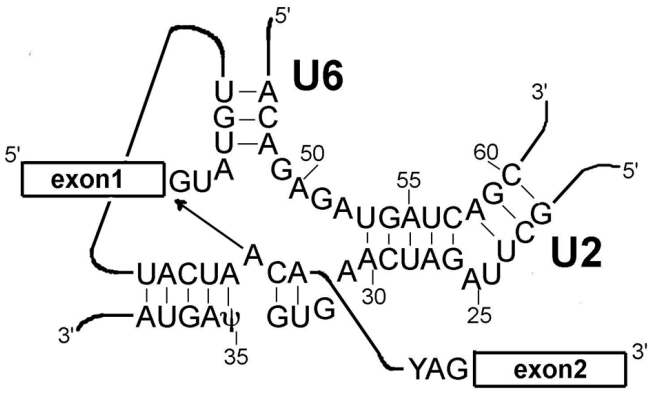

Figure 1. Pairing of U2 snRNA with the branch site sequence of the intron results in the bulging of the adenosine residue responsible for nucleophilic attack at the 5' splice site. Sequences shown are from *S. Cerevisiae*.

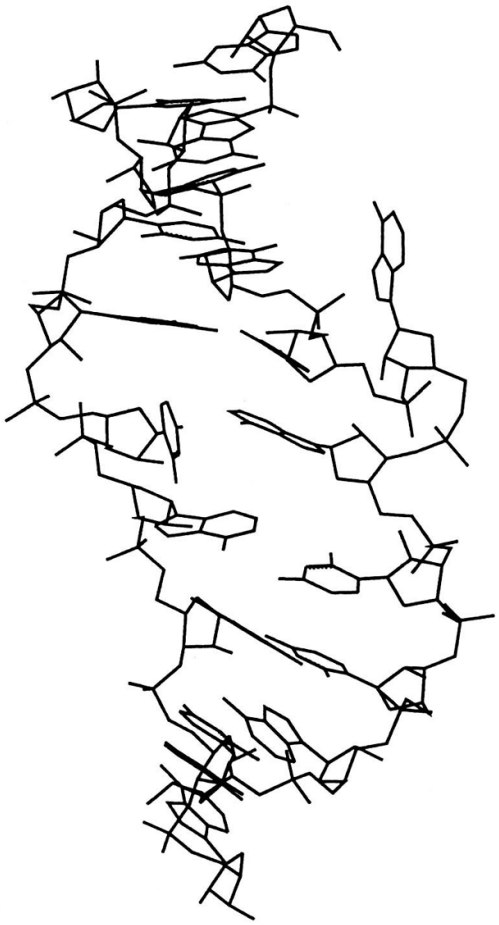

Figure 2. Structure of the modified U2 snRNA-intron pairing containing the conserved pseudouridine. One of a family of low energy structures generated using X-PLOR 3.1 and visualized utilizing the program INSIGHT is shown.

the unmodified analog. Data from NMR spectra of non-exchangeable protons in the unmodified construct demonstrated A-form helical geometry and continuous base-stacking throughout the molecule. Incorporation of ψ at the conserved position, however, was accompanied by a marked deviation from helical parameters and an extrahelical orientation for the unpaired adenosine base (Fig. 2). Incorporation of ψ also stabilized the branch site interaction, contributing -0.5kcal/mol to duplex ΔG^{O}. These findings suggest that the presence of this conserved pseudouridine base induces a change in the structure and stability of the branch site sequence, and imply that the extrahelical orientation of the branch site adenosine may facilitate recognition of this base during spliceosome assembly.

High Field EPR Study of Heme Proteins Radical Intermediates

Pogni, R., Univ. of Siena, Italy, Chemistry
Maniero, A.L., Univ. of Padova, Italy, Physical Chemistry
Brunel, L.-C., NHMFL

The reaction of heme proteins with H_2O_2 and related species continues to attract considerable attention. While hemoglobin and/or myoglobin are not primarily catalytic proteins, it has been demonstrated that they possess peroxidase-like activity.[1-3] Similar to classical peroxidases, such as horseradish peroxidase, hemoglobin reductively cleaves hydrogen peroxide, retaining one of the oxidizing equivalents on the iron of the heme in the form of an oxo-ferryl species (Fe^{IV}=O). However, the second oxidizing equivalent is located on the globin as a free radical.[4,5] This is different from the classical horseradish peroxidase, where the second oxidizing equivalent is the porphyrin IX cation radical.[6] Gunther *et al.*[1] have shown that the initial reaction of H_2O_2 with Fe^{3+} myoglobin results in the formation of a tryptophan-derived radical which can be trapped with the spin-trap DBNBS. The analysis of the anisotropic X band EPR spectra obtained was aided by proteolytic digestion of the protein to release low molecular weight fragments containing the radical adduct; these fragments give rise to isotropic spectra which are identical to those seen with low molecular weight tryptophan-containing materials. In a recent paper,[7] the protein radical for hemoglobin and cytochrome c was trapped using methyl-nitrosopropane (MNP) and information on magnetic and dynamic parameters of the complexes were obtained by simulation of the slow motional X band EPR spectra.

However, many X band EPR studies have pointed out that different amino acid residues must be involved in the process. High Field EPR can contribute to elucidating the nature and origin of these protein radicals.

HF EPR measurements have been performed on hemoglobin and cytochrome c oxidized with H_2O_2. Spectra have been recorded at frequencies of about 110, 220, and 330 GHz, increasing the temperature from 4 K to 100 K. Except for the decrease in the signal to noise ratio, the main spectral features don't change in the examined temperature range. Examples of experimental and simulated spectra of the oxidized hemoglobin at different microwave frequencies are reported in the figure.

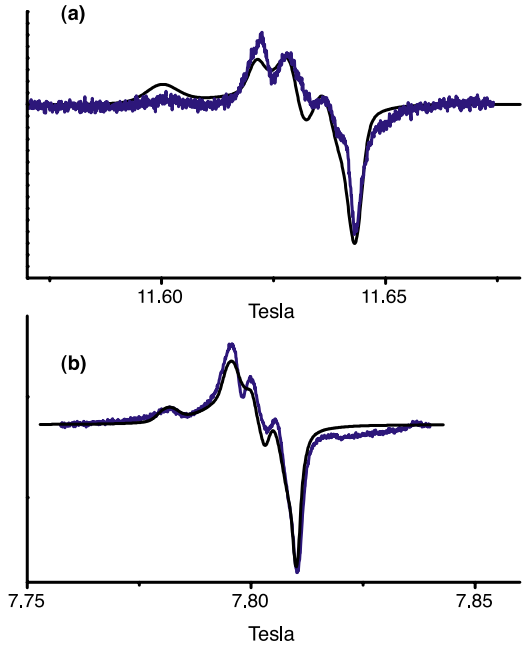

Figure 1. HF-EPR spectra at T=10 K of hemoglobin oxidized with H_2O_2, recorded at **(a)** ν=330 GHz and **(b)** ν=220 GHz. Simulated spectra, shown in the figures, are obtained from the superposition of signals due to two different radical species.

For both the systems studied (hemoglobin and cytochrome c), the HF EPR spectra can be interpreted as due to the presence of at least two different radical species. On the basis of the g tensors obtained from the spectral simulation, these can be identified as radicals centered on a tyrosine and on a tryptophan residues.

[1] Gunther, M.R., *et al.,* J. Biol. Chem., **270** (27), 16075-16081 (1995).
[2] Kelman, D.J., *et al.,* J. Biol. Chem., **269** (10), 7458-7463 (1994).
[3] Davies, M.J., Biochim. Biophys. Acta, **10,** 77, 86-90 (1991).
[4] Harada, K., *et al.*, J. Biochem., **101**, 283-286 (1987).
[5] King, N.K., *et al.,* J. Biol. Chem., **238**, 1520-1528 (1963).
[6] Roberts, J.E., *et al.,* J. Biol. Chem., **256**, 2118-2121 (1981).
[7] Pogni, R., *et al.,* Int. J. of Quantum Chem., **73**, 249-254 (1999).

The *G*-Factor Anisotropy of Bacteriochlorophyll $a^{\bullet+}$

Poluektov, O., Argonne National Laboratory
Thurnauer, M., Argonne National Laboratory
Brunel, L.-C., NHMFL
Zvyagin, S., NHMFL
Boyce, C., Univ. of South Carolina, Biology
Walker, L., NHMFL/UF, Chemistry
Angerhofer, A., NHMFL/UF, Chemistry

Bacteriochlorophyll *a* (BChl *a*) is the main pigment in the photosynthetic system of most purple photosynthetic bacteria. It serves both as the main energy carrying component of the antenna complexes as well as the primary donor in the photosynthetic reaction center protein (RC). The anisotropic *g*-tensors of chlorophyll radicals have received quite a bit of attention recently due to the possibility to (a) measure them accurately with EPR in very high magnetic fields,[1-3] and (b) the relatively high accuracy with which they can be predicted theoretically.[3] Here we report the EPR spectrum of fully deuterated BChl *a* at a field of 11.6 T and a frequency of 325.158 GHz (Fig. 1). Clearly, the three main peaks representing the principal components of the *g*-tensor are visible in the spectrum. A simulation resulted in the following values: g_{xx}=2.00338, g_{yy}=2.00256, and g_{zz}=2.00217, with a relative error margin of ± 0.00005. The phase of the spectrum is distorted due to rapid passage effects common to high-field EPR. Nevertheless, the simulation allows the accurate determination of the principal components of the *g*-tensor.

The anisotropy in the x,y-plane is more pronounced than for plant chlorophyll $a^{\bullet+}$, as expected due to the saturation of a double bond on the second pyrrole ring in BChl *a* which increases the in-plane asymmetry of the conjugated π-system. As with plant chlorophyll *a,* the spectral resolution of the principal components of the *g*-tensor is only present for fully deuterated material as *g*-strain is present in the organic solvent matrix (frozen methylene chloride at 5 K). The accurate determination of the *g*-tensor components of monomeric BChl $a^{\bullet+}$ helps to understand the *g*-anisotropy of the primary donor radical cation and its dimer character, and thus helps in the correct interpretation of W-band and D-band time-resolved spectra of the radical pair in photosynthetic reaction centers.[4]

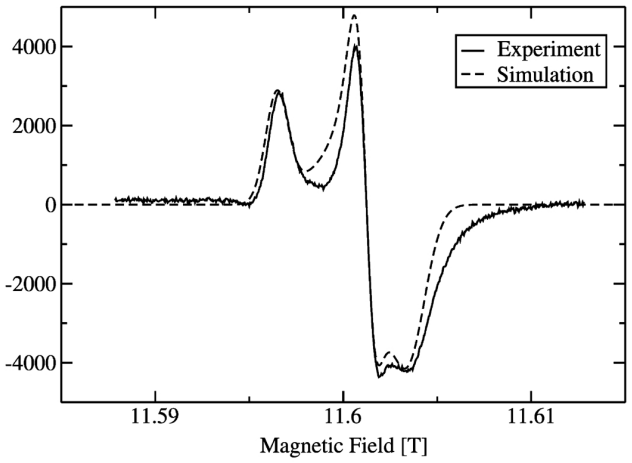

Figure 1. EPR spectrum and computer simulation of the BChl $a^{\bullet+}$ radical cation in methylene chloride at 5 K. Fully deuterated BChl was used.

[1] Bratt, P.J., *et al*., J. Phys. Chem. B, **101**, 9686 (1997).
[2] Bratt, P.J., *et al*., J. Phys. Chem. B, **103**, 10973 (1999).
[3] Bratt, P.J., *et al*., J. Phys. Chem. B, **104**, 6973 (2000).
[4] Berthold, T., *et al*., J. Phys. Chem. B, **103**, 10733 (1999).

Active-Site Structures of ATP-Utilizing Enzymes

Ray, B.D., Indiana Univ. Purdue Univ. Indianapolis, Physics
Rao, B.D.N., IUPUI, Physics

We continue to utilize the 720 MHz NMR spectrometer at the NHMFL for our project characterizing the "Active-Site Structures of ATP-Utilizing Enzymes" (funded by NIH GM43966). A critical part of this project is the determination of the distances between activating substituent paramagnetic cations (Mn(II) or Co(II)) and selected ^{13}C, ^{15}N, and ^{31}P nuclei located in the substrates bound at the active sites of these enzymes, based on the enhancement in the spin-lattice relaxation rates of the nuclei due to the presence of the paramagnetic cations in their vicinity. In order to properly analyze the relaxation data and evaluate the distances, the data must be acquired at least at three different nuclear Larmor frequencies. We make measurements on the 300 MHz and 500 MHz spectrometers available with us, and make a third set of measurements on the 720 MHz machine located at the NHMFL.

During the year 2000, in collaboration with Professor Honggao Yan of Michigan State University, we initiated similar measurements on a new enzyme, guanylate kinase, and on the Y78F mutant of that enzyme. Also, in collaboration with Dr. Vidya Raghunathan at the National Institute of Immunology, New Delhi, India, we initiated measurements on two isoforms of 3-P-glycerate kinase from Leishmania mexicana, PGKB, and PGKC. We have made one visit during September 2000, and another is planned for January 2001. It is anticipated that some of the results of these experiments will be reported in the next year or two.

Stable Isotope Incorporation Triples the Upper Mass Limit for Determination of Elemental Composition by Accurate Mass Measurement

Rodgers, R.P., NHMFL
Blumer, E.N., NHMFL
Hendrickson, C.L., NHMFL
Marshall, A.G., NHMFL/FSU, Chemistry

By comparing electrospray ionization FT-ICR mass spectra and collision-induced dissociation (CID) FT-ICR mass spectra of a phospholipid (851 Da) extracted from natural-abundance and 99% ^{13}C bacterial growth media, we are able to reduce its number of possible elemental compositions (based on ±10 ppm externally calibrated mass accuracy and biologically relevant compositions[1] constraints) from 394 to 1. The basic idea is simply that the mass of a molecule containing N carbon atoms increases by N Da when ^{12}C is replaced by ^{13}C. Once the number of carbons is known, the number of possible combinations of *other* atoms in the molecule is greatly reduced. We demonstrate the method for a stored-waveform inverse Fourier transform-isolated phospholipid from an extract of membrane lipids from *Rhodococcus rhodochrous* hydrocarbon-degrading bacteria grown on either natural abundance or 99% ^{13}C-enriched mixtures of *n*-hexadecane and *n*-octadecane. We project that this method raises the upper mass limit for unique determination of elemental composition from accurate mass measurement by a factor of at least three, thereby extending "chemical formula" determination to identification and sequencing of larger synthetic and bio-polymers: phospholipids, oligopeptides of more than 3-4 amino acids, DNA or RNA of more than 2 nucleotides, oligosaccharides of more than 3 sugars, etc. The method can also be extended to determination of the number of other atoms for which heavy isotopes are available (e.g., ^{15}N, ^{34}S, ^{18}O, etc.).

Acknowledgements: The authors thank Daniel McIntosh for machining all of the custom parts required for the 9.4 T instrument construction and John P. Quinn for many helpful discussions. This

work was supported by the NSF National High-Field FT-ICR Mass Spectrometry Facility (CHE-94-13008), American Chemical Society Division of Analytical Chemistry graduate fellowship (to RPR) sponsored by the Society of Analytical Chemists of Pittsburgh, FSU, and the NHMFL.

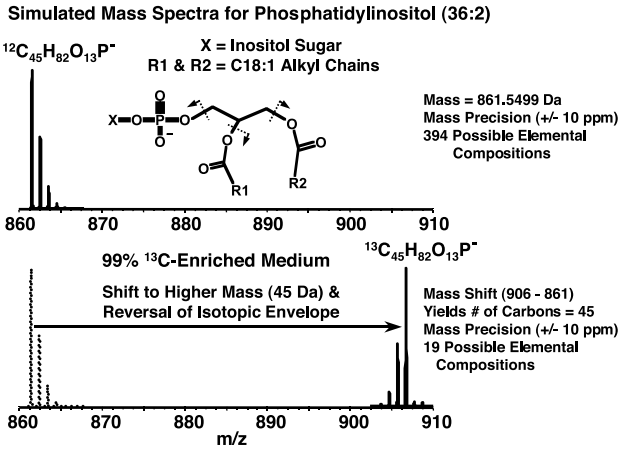

Figure 1. Simulated mass spectra for natural abundance (top) and 99% ^{13}C -enriched (bottom) 36:2 phosphatidylinositol anion. At a mass accuracy of ±10 ppm, the number of possible elemental compositions is 394. Prior knowledge of the number of carbon atoms in the patent lipid anion reduces the number of possible elemental compositions by a factor of ~20, thereby simplifying the assignment of the chemical formula for the lipid.

[1] Rodgers, R.P., *et al*., Environ. Sci. & Technol., **34**, 535-540 (2000).

[2] Rodgers, R.P., *et al*., J. Am. Soc. Mass Spectrom., **11**, 835-840 (2000).

Structural Features of the Branch Site from the Group II Self-Splicing Intron Studied by ^{1}H NMR

Schroeder, K.T., NHMFL/FSU, Chemistry
Newby, M.I., NHMFL/FSU, Chemistry and Molecular Biophysics
Greenbaum, N.L., NHMFL/FSU, Chemistry and Molecular Biophysics

Messenger (m)RNAs, as part of their maturation processes, undergo removal of noncoding regions (introns) and ligation of the remaining sequences (exons). Certain RNA sequences, known as self-splicing introns, are capable of catalyzing their own removal from nascent mRNA transcripts. The self-splicing event is initiated by the 2'OH of a conserved adenosine residue, termed the branch site, which resides in Domain 6. This project examines the structural features of the branch site region from intron aI5γ of the yeast mitochondrial COXI gene, a Group II self-splicing intron, by solution NMR spectroscopy.

Domain 6 of the Group II intron is a stem loop containing an internal loop and the unpaired branch site adenosine. We have obtained two constructs representing Domain 6: a 37-nucleotide oligomer, and an abbreviated 25-mer that does not contain the internal loop (Fig. 1). Both sequences include two non-Watson-Crick G-U base pairs flanking the unpaired adenosine. NMR studies have shown the internal loop of the 37-mer to be unstructured in the absence of Mg^{2+} and more structured in its presence, and that it is structurally independent of the region including the branch site adenosine. Preliminary assignment of exchangeable and non-exchangeable protons in NOESY spectra of the 25-mer indicate a predominantly A-form helical structure. The downfield position of the resonance assigned to the H8 proton of A18, at 8.2 ppm (Fig. 2), the branch site adenosine, indicates that this proton is not very shielded, suggesting an extrahelical orientation.

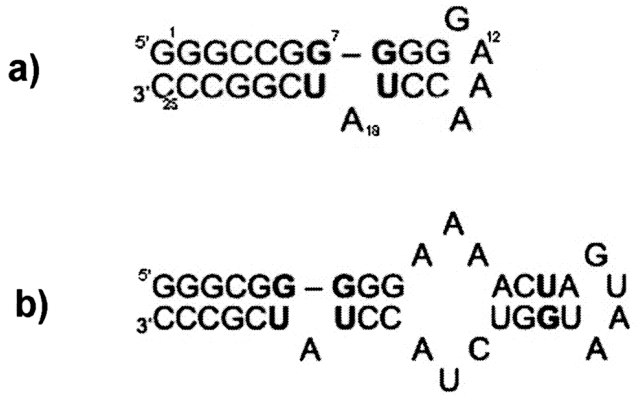

Figure 1. The 37-mer (a) is the analogous structure of the Group II Domain 6-stem loop. The 25-mer (b) is the abbreviated Group II Domain 6 from which the internal loop has been deleted.

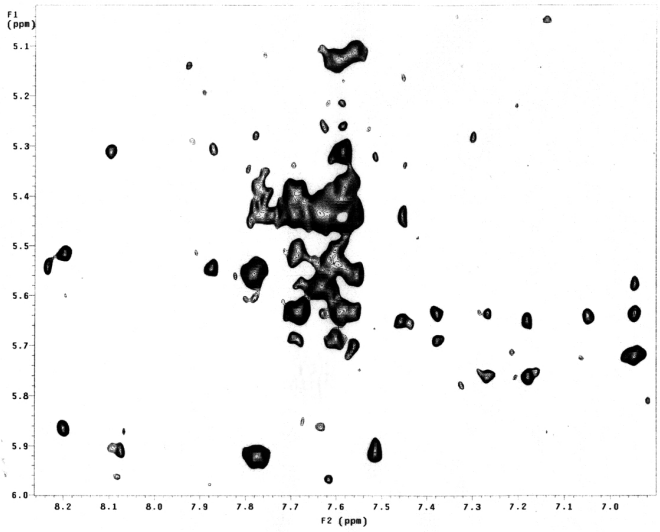

Figure 2. Anomeric-aromatic region of a NOESY spectrum of the non-exchangeable protons in the abbreviated Group II Domain 6 constructs. The sample is approximately 0.8 mM RNA in 10 mM sodium phosphate, 50 mM sodium chloride, and 0.1 mM EDTA in D_2O, pH 6.4. The spectrum was acquired at 10° C on the 500 MHz spectrometer at the NHMFL, with a mixing time of 400 msec.

NMR Studies of Spinal Cords *In Vivo* and *In Vitro*

Silver, X.S., UF, Biochemistry and Molecular Biology
Inglis, B.A., UF McKnight Brain Institute
Bossart, E.L., UF, Physics
Vemuri, B., UF, Computer and Information Science and Engineering
Anderson, D.K., UF, Neuroscience
Reier, P.J., UF McKnight Brain Institute/UF, Neuroscience
Beck, B.L., UF, NHMFL
Mareci, T.H., UF McKnight Brain Institute/UF, Biochemistry and Molecular Biology/NHMFL

A major focus of our group at UF is the use of MR to assess and monitor spinal cord injury in animal models and evaluate the effectiveness of neuroprotective agents and methods to repair injured spinal cords. This project has required the development of MR hardware, as well as measurement techniques and methods of data processing, and continues with studies on the effectiveness of cellular transplantation as a means of repairing injured spinal cords. As part of this work, we reported[1] the measurement of multiple-diffusion rates in the spinal cord. Over the last year, we have extended our studies to include diffusion tensor mapping of the two diffusion-rate regimes in the spinal cord.[2] In collaboration with Barbara Beck, we developed a system of phased-array coils for cat spine imaging at 4.7 T. Further improvements in the development of inductively coupled implanted coils have involved a study of the resonance mode selection to optimize sensitivity.[3] Other new developments include a study of blood-spinal-cord barrier disruption following injury[4] and a new collaboration with Dr. Baba Vemuri of the computer science department of UF to use diffusion tensor measurements to map fiber tracts in spinal cord white matter.

Most recently, we have been developing the use of the new 750 MHz wide bore instrument for these studies and have obtained excellent three dimensional images as shown in Fig. 1. We shall be using this instrument in our future studies.

Figure 1. 3D MR image of an isolated rat spinal cord obtained at 750 MHz. Image is a multiple-slice single spin echo with TR/TE = 2500/16, 8 averages (total time, ~ 43 minutes), matrix 128 x 128 x 48, FOV 5 x 5 x 5.76 mm (120 micron thick slices), giving a resolution ~ 39 x 39 x 120 microns per voxel.

Acknowledgements: Thanks to the following for funding: NHMFL, NIH, State of Florida, and the Brain and Spinal Cord Injury Research Trust Fund.

[1] Bossart, E. *et al*, Proceedings of the ISMRM, Denver, (2000).
[2] Inglis, BA, *et al.,* in press, *Magn. Reson. Med.*, 2001.
[3] Mareci, T.H., *et al*., submitted to ISMRM (2001).
[4] Mareci, T.H., *et al*., submitted to ISMRM (2001).

High Frequency and Field EPR Spectroscopy of a Mononuclear Manganese(II) Enzyme, FosA, Involved in Bacterial Drug Resistance

Telser, J., Roosevelt Univ., Chemistry
Smoukov, S., Northwestern Univ., Chemistry
Hoffman, B.M., Northwestern Univ., Chemistry
Bernat, B.A., Vanderbilt Univ., Biochemistry
Armstrong, R.N., Vanderbilt Univ., Biochemistry
Krzystek, J., NHMFL
Brunel, L.-C., NHMFL

FosA is a manganese metalloglutathione transferase that confers resistance to the broad-spectrum antibiotic fosfomycin, (1*R*,2*S*)-epoxypropylphos-phonic acid.[1,2] The active enzyme is a dimer of 16 kDa subunits, each of which contains one mononuclear Mn^{2+} site. Such an active site is relatively unusual in metalloenzymes. X-band EPR spectroscopic studies on FosA have already been published[2] and show a signal characteristic of Mn^{2+} ($3d^5$, S=5/2), similar to that for $[Mn(H_2O)_6]^{2+}$. FosA in the presence of excess fosfomycin (i.e., the drug-enzyme complex), however, does not exhibit an X-band spectrum at 77 K, which could either be the result of oxidation to Mn^{3+} ($3d^4$, S=2; often "EPR-silent" at X-band), or retention of Mn^{2+}, but with significantly different EPR properties, especially relaxation rates.

Both FosA (denoted E.Mn^{2+}) and FosA in the presence of fosfomycin (denoted E.Mn^{2+}.S) have been studied at Northwestern using 35 GHz EPR at 2 K. EPR spectra from both enzyme complexes were observed.[3] Analysis of these EPR spectra shows that a profound change in the electronic parameters of Mn^{2+} occurs upon interaction with fosfomycin: the axial zero-field splitting changes from $|D| = 0.06$ cm^{-1} to 0.23 cm^{-1}.

Preliminary HFEPR results have been obtained at the NHMFL on E.Mn^{2+}.S, the sample of greatest interest. A representative spectrum recorded at 189.6 GHz is shown in Fig. 1. The specific sample preparation was not optimized for maximum Mn^{2+} to enzyme, or fosfomycin to enzyme, binding. As a result, there is a dominant signal which may be due to $[Mn(H_2O)_6]^{2+}$ and/or E.Mn^{2+}. Nevertheless, several important conclusions can be drawn from this preliminary result. First, it is possible to observe HFEPR from a small amount (~ 50 μL) of a frozen aqueous solution of a metalloprotein in millimolar concentration. Second, there are no signals attributable to Mn^{3+}, corroborating the conclusion of no oxidation of manganese occuring upon fosfomycin binding. HFEPR has been shown to be very sensitive to "EPR-silent" Mn^{3+}, both in the solid state, and in solution.[4] Third, as shown in studies by Freed and co-workers,[5,6] analysis of Mn(II) spectra with relatively large zero-field splitting is greatly simplified at high fields, allowing more accurate determination of magnitude and sign. This analysis is in progress, but qualitative inspection of Fig. 1 suggests that the spread of the outer signals, likely due to E.Mn^{2+}.S, should give a direct measure of D. Optimally prepared samples will soon allow a more quantitative analysis.

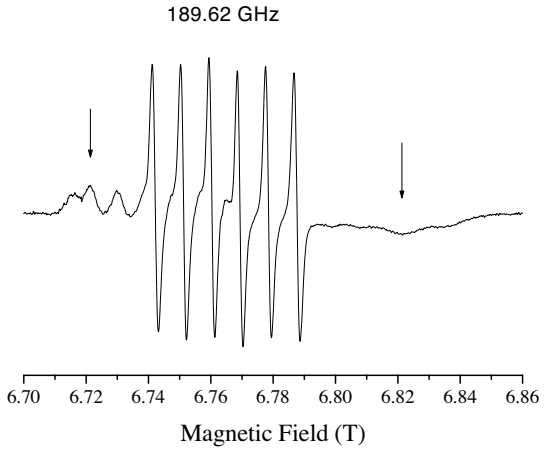

Figure 1. 189.62 GHz HFEPR spectrum of FosA in the presence of fosfomycin (E.Mn^{2+}.S) at T=15 K. The sample preparation has not been optimized to yield a maximum binding of either Mn^{2+} to enzyme, or of fosfomycin to enzyme. The central sextet may be due to free Mn^{2+} or to E.Mn^{2+}. However, the features at fields above and below the sextet (arrows) are likely due to E.Mn^{2+}.S, which has larger zero-field splitting.

[1] Armstrong, R.N., Chem. Res. Toxicol., **10**, 2-18 (1997).
[2] Bernat, B.A., *et al.,* Biochemistry, **36**, 3050-3055 (1997).
[3] Smoukov, S., *et al.,* Manuscript in preparation.
[4] Krzystek, J., *et al.,* Inorg. Chem., **38**, 6121-6129 (1999), and *2000 NHMFL Annual Research Review.*
[5] Lynch, W.B., *et al.,* J. Am. Chem. Soc., **115**, 10909-10915 (1993).
[6] Wood, R.M., *et al.,* Inorg. Chem., **38**, 5384-5388 (1999).

NMR Studies of Red Blood Cell Ghosts

Thelwall, P., UF McKnight Brain Institute/UF, Neuroscience
Blackband, S., UF McKnight Brain Institute/UF, Neuroscience/NHMFL

Studies of a variety of tissues using diffusion MRI have opened up the potential of diffusion techniques for determining the compartmental structure of the tissues. However, even the simplest systems are still complicated to model and limited in the ability to control and vary the system. To further develop these issues, we have most recently explored the red blood cell ghost model for constructing testable systems for our modeling procedures. In short, red blood cells are processed in a way to extract the intracellular components to form cellular "bags."

With this model, we are able to control and manipulate the intra- and extracellular content, cell size, cell density, and membrane permeability to water, to form a controlled two-compartment system. As an example, we have performed a preliminary study examining the diffusion characteristics of the blood cell ghosts as a function of hypo and hypertonic perturbation. Fig. 1 shows the diffusion curves again, clearly demonstrating shifts in the diffusion curves with cell swelling and shrinking. When fitted to a biexponential fast and slow ADC component, data can again be generated and show that the fraction of the fast component and D_{fast} decrease with cell swelling as we expected. Further experimentation, as a function of cell density, diffusion time, and cell content are required to further illucidate the mechanisms of these changes, and similar experiments are required on the single cells and brain slices. The results can then be used in the generation of the mathematical models. A preliminary account of these new studies have been submittd to a meeting[1] and a manuscript is in preparation.

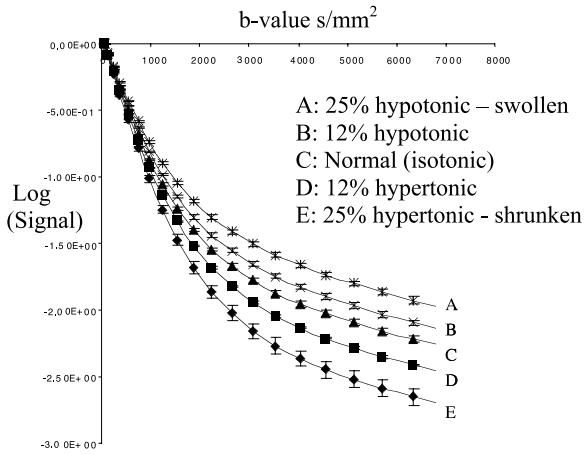

Figure 1. Diffusion curves of red blood cell ghosts as a function of cell swelling and shrinkage at 300 mOsm and a cell density of 50%.

Acknowledgements: This work was supported by the NHMFL, the NIH, and the UF McKnight Brain Institute.

[1] Thelwall, P., *et al.,* submitted to, Proc. of the ISMRM (2001).

Structural Insight into Intact M2 Membrane Protein From Influenza A Virus by 2D Pisema Solid State NMR

Tian, C., NHMFL/FSU, Molecular Biophysics
Tobler, K., Northwestern Univ., Biochemistry, Molecular Biology, and Cell Biology
Lamb, R.A., Northwestern Univ., Biochemistry, Molecular Biology, and Cell Biology
Cross, T.A., NHMFL/FSU, Chemistry and Molecular Biophysics

The influenza A virus M2 integral membrane protein is an ion channel that permits protons to enter virus particles during the uncoating of virions in the endosomes. The protein also modulates the pH of the trans-Golgi network in virus-infected cells. The 97 amino acid residues M2 protein forms a homotetramer to fulfill the function of a proton channel.

The intact M2 protein has been expressed, purified, and reconstituted into a DMPC/DMPG liposome. CD spectrum of the intact M2 protein in detergent micelles has shown that 67% of the sequence is alpha helical.

The uniformly ^{15}N labeled intact M2 protein and ^{15}N-Val, ^{15}N-Leu amino acid labeled intact M2 protein have been expressed with defined M9 media and the labeling has been confirmed by HSQC solution NMR experiments.

The reconstituted intact M2 DMPC/DMPG proteoliposome has been prepared in uniformly oriented solid state NMR samples for the PISEMA experiment. The PISEMA spectra of ^{15}N uniformly labeled intact M2 protein and ^{15}N-Val amino acid specific labeled intact M2 protein in lipids have been obtained. The spectra (Fig. 1) show that there is only one transmembrane part present in the intact M2 protein, and it also shows single axial symmetry in the functional homotetramer protein, which have been suggested by many other research groups based on their electrophysiology experiments and mutagenesis scanning experiments.

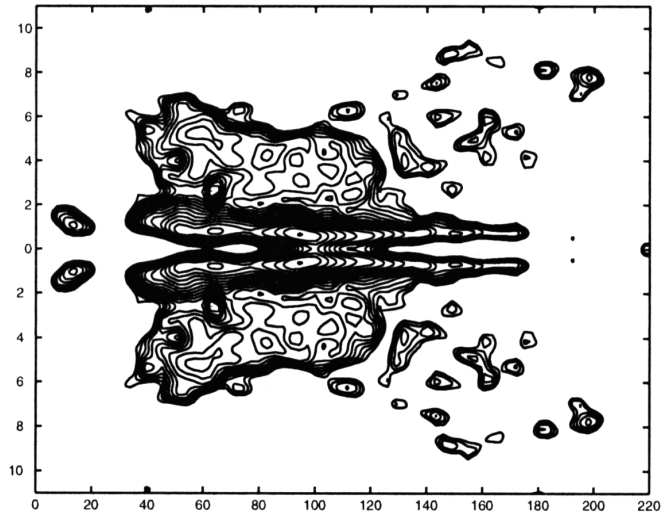

Figure 1A. PISEMA spectrum of ^{15}N uniformly labeled intact M2 protein in DMPC/DMPG. The sample has been uniformly oriented on glass slides. The PISEMA experiments were run on 400 MHz wide bore NMR spectrometer with 5.59 µs pulse width on H channel and 6.0 µs on ^{15}N channel. Data was acquired with 32 FIDs and 256 sampling points under 50 KHz proton decoupling. Data was processed with 100 Hz linebroading and sinebell on both dimensions by home-developed MATLAB scripts.

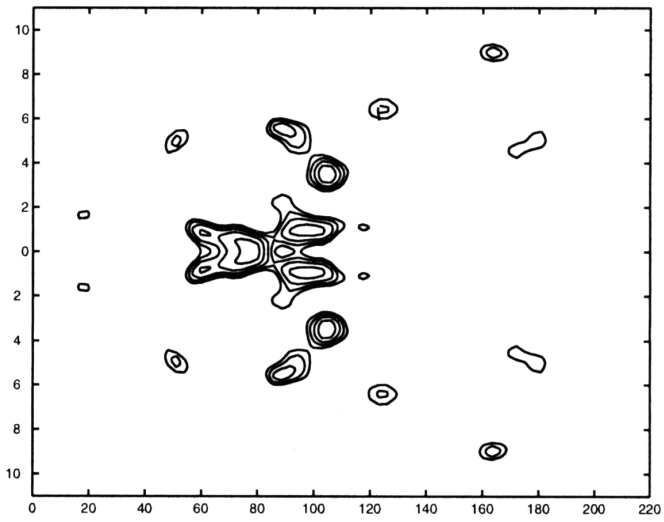

Figure 1B. PISEMA spectrum of ^{15}N Val labeled intact M2 protein in DMPC/DMPG. The sample preparation and data processing are the same as the above. Data was acquired with 24 FIDs with 256 sampling points under 50 KHz proton decoupling.

[1] Grambas, S., *et al*., Virology, **191**, 541-549 (1992).
[2] Schroeder, C., *et al*., Journal of General Virology, **75**, 3477-3484 (1994).
[3] Holsinger, L.J., *et al*., Journal of Virology, 1551-1563 (1944).
[4] Chizhmakov, I.V., *et al*., Journal of Physiology, **494**, 329-336 (1996).

A Disorder-to-Order Transition in the Regulation of Diphtheria Toxin Repressor Activity

Twigg, P.D., FSU, Molecular Biophysics
Parthasarathy, G., FSU, Molecular Biophysics
Guerrero, L., FSU, Molecular Biophysics
Logan, T.M., FSU, Chemistry
Caspar, D.L.D., FSU, Biology

Diphtheria toxin repressor (DtxR), a 226-amino acid protein, is an iron-dependent negative regulator of genes in *Corynebacterium diphtheriae,* which code for iron-uptake and oxidative stress-associated proteins, and for the corynephage encoded diphtheria toxin. Solution nuclear magnetic resonance spectra of DtxR demonstrate that while the C-terminal domain (residues 149-226) of the protein is well-ordered, the N-terminal domain (residues 1-130) exhibits conformational flexibility, and exists as an ensemble

of structures in chemical exchange with each other. Binding of divalent metal cations induces a dramatic conformational reorganization to a more ordered state as evidenced by changes in the NMR spectra.

2-dimensional HSQC spectra were collected on uniformly ^{15}N-labelled DtxR(C102D) at 30° C. Surprisingly, the spectra contained only resonances that were assignable to the C-terminal domain by inspection. There were very few additional resonances that could be tentatively assigned to the N-terminal portion. In general, the structure of the C-terminal domain was quite similar in the C-terminal domain construct DtxR(130-226). Electrophoretic mobility and rigorous removal of contaminating metal showed that proteolytic degradation and paramagnetic metal ion binding were not the source of the missing resonances. The most plausible explanation was that the entire N-terminal domain was undergoing conformational exchange on an intermediate NMR time-scale, resulting in severe resonance broadening. HSQC spectra were collected at 4° C to shift the position of conformational equilibrium, with the resulting appearance of numerous resonances that are not from the C-terminal domain and are presumed to be from the N-terminal domain (Fig. 1). We have not completed resonance assignments for this spectrum at this time, but it is apparent that two classes of resonances are observed. Some resonances are quite sharp, and shifted away from random coil positions, indicating the presence of some defined structure in the N-terminal domain at 4C. A second class of resonances are clustered around the random coil region of the spectrum, and exhibit broader lines, indicating that some portion of the NTD is still undergoing some conformational exchange.

Interestingly, we observe additional significant changes in the 2D HSQC spectrum upon addition of a diamagnetic divalent metal, Cd^{2+} (Fig. 1). Specifically, we see a substantial sharpening of many resonances and a shifting of many resonances away from the random coil region, indicating a structural transition that is induced by metal ions.

We propose that this disorder-to-order structural transition observed in solution is involved in regulating the monomer-dimer equilibrium in DtxR. This structural transition better explains the available data on regulation of DtxR than existing crystal structures.

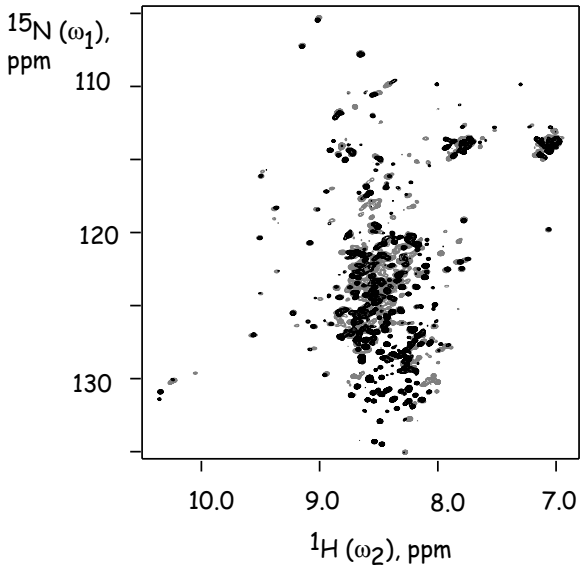

Figure 1. Overlay of HSQC spectra of DtxR at 4C in the presence (dark circles) and absence (light circles) of Cd^{2+}.

Magnetic Field Manipulation of Cell Division

Valles, Jr., J.M., Brown Univ., Physics
Mowry, K.L., Brown Univ., Molecular Biology, Cell Biology, and Biochemistry

The application of a high static magnetic field to embryos of the frog, *Xenopus laevis*, dramatically alters the geometry of their early cell divisions. As shown in the upper panels of the figure, the nominally horizontal planes of the third cell divisions become vertical in high magnetic field exposed embryos. This year, we used confocal microscopy and immunocytochemistry to visualize internal molecular structures involved in cell division to derive new insight into this effect. The lower panels in the figure show side views of two eggs that were fixed as the third cell division was occurring, cut in half, and treated to reveal the microtubules in the mitotic apparatus (MA) and the chromosomes in fluorescence (see arrows). The lower panel images are rotated about 30 degrees counterclockwise from the images

in the upper panels. Notice that the orientation of the long axes of these bright regions differ by 90 degrees between the two images. The "vertical" orientation in the left panel corresponds to that expected for the cell to divide with a horizontal division plane, while the "horizontal" orientation in the right panel corresponds to that expected for the cell to divide with a vertical division plane. The MA's in virtually all eggs exposed to 22 T were tilted by more than 45 degrees from the nominally vertical orientation of the MA's in the controls. This result implies that the altered cell division geometries result from a magnetic field induced reorientation of the MA. While the exact mechanism for the MA reorientation has not yet been determined, the capability to manipulate its orientation with magnetic field may be useful as a tool for investigating fundamental questions in cell division.

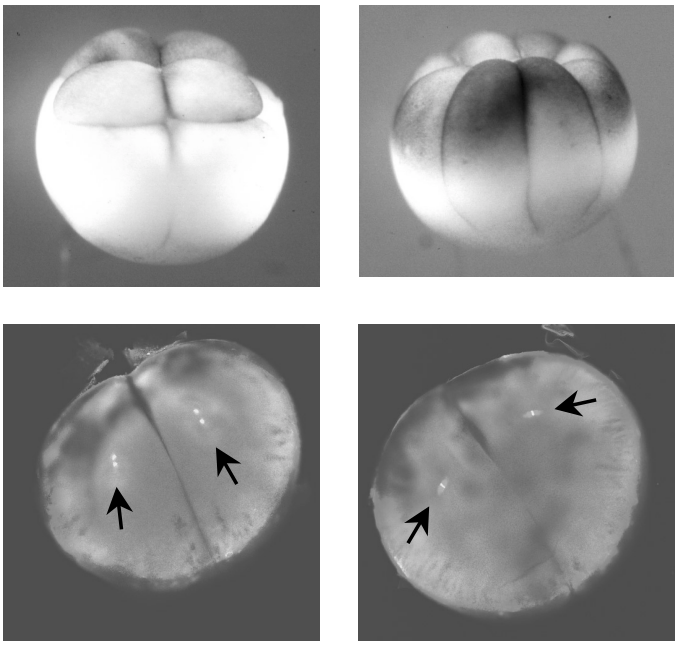

Figure 1. ***Upper panels:*** Side views of control (left) and magnetic field exposed (right) (17 T) eight cell embryos. The left embryo shows the nominal cell division pattern. In contrast, the third cell divisions in the field exposed embryo (right) resulted in vertical, rather than horizontal planes. ***Lower panels:*** Images of third cell cycle mitotic apparatuses in control (left) and magnetic field (right) (22 T) exposed embryos. The arrows point at the mitotic apparatuses, which are composed of microtubules and chromosomes, in each of the cells. Note that the orientation of the long axis of these structures differs between the two images. Their orientations correlate directly with the cell division patterns shown in the upper panels.

Acknowledgements: This work was done in collaboration with J. Edwardson, C. Schweidenback, and J. Denegre. NSF MCB No. 98-16986 also supported this work.

Gas-Phase Cleavage of PTC-Derivatized Electrosprayed Tryptic Peptides in an FT-ICR Trapped-Ion Cell: Mass-Based Protein Identification without Liquid Chromatographic Separation

van der Rest, G., NHMFL
He, F., NHMFL
Emmett, M.E., NHMFL
Marshall, A.G., NHMFL/FSU, Chemistry
Gaskell, S.J., University of Manchester Institute of Science and Technology, Michael Barber Centre for Mass Spectrometry, Chemistry

Condensed-phase protein sequencing typically relies on N-terminal labeling with phenylisothiocyanate ("Edman" reagent), followed by cleavage of the N-terminal amino acid. Similar Edman degradation has been observed in the gas phase by collision-activated dissociation of the N-terminal phenyl thiocarbamoyl protonated peptide [*J. Mass Spectrom.* 1997, *32*, 225-231] to yield complementary b_1 and y_{n-1} fragments, identifying the N-terminal amino acid. By use of infrared multiphoton (rather than collisional) activation, and Fourier transform ion cyclotron resonance (rather than quadrupole) mass analysis, we extend the method to direct analysis of a mixture of tryptic peptides. We validate the approach with bradykinin as a test peptide, and go on to analyze a mixture of 25 peptides produced by tryptic digestion of apomyoglobin. A b_1^+ ion is observed for three of the Edman-derivatized peptides, thereby identifying their N-terminal amino-acids. Search of the SWISSPROT database gave a single hit (myoglobin, from the correct biological species), based on accurate-mass FT-ICR MS for as few as one Edman-derivatized tryptic peptide. The method is robust—it succeeds even with partial tryptic digestion, partial Edman derivatization, and partial MS/MS IRMPD cleavage. Improved efficiency and automation should be straightforward.

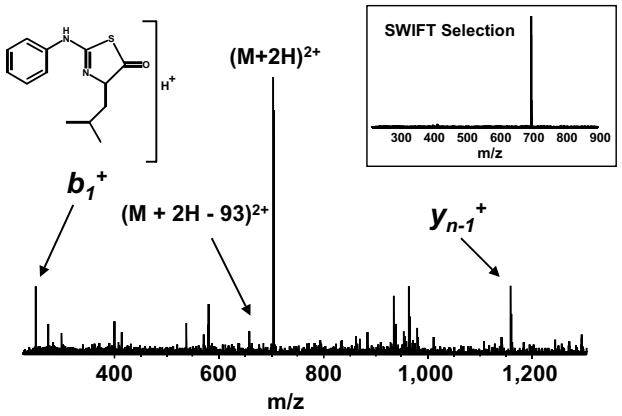

Figure 1. FT-ICR mass spectrum following IRMPD fragmentation (5 s laser irradiation) of the SWIFT isolated (see inset) (PTC)L32-K42^{2+} derivatized peptide from trypsin-digested myoglobin. The N-terminal amino acid is clearly identified from the b_1 fragment ion.

Acknowledgements: We thank Christopher L. Hendrickson for helpful discussions. This work was supported by the NSF National High Field FT-ICR Facility (CHE-99-09502), FSU, and the NHMFL. Work at UMIST is supported by the UK Biotechnology and Biological Sciences Research Council under COGEME (the Consortium for the Functional Genomics of Microbial Eukaryotes) and by the Defence Evaluation and Research Agency (DERA).

[1] van der Rest, G., *et al.*, "Gas-Phase Cleavage of Edman-Derivatized Electrosprayed Tryptic Peptides: Mass-Based Protein Identification without Liquid Chromatographic Separation," J. Am. Soc. Mass Spectrom., **12**, 0000-0000 (2001).

NMR Studies of Two Proteins That Affect Tissue Remodeling in Human Health and Disease

Van Doren, S.R., Univ. of Missouri-Columbia, Biochemistry
Gao, G., Univ. of Missouri-Columbia, Biochemistry
Arumugam, S., Univ. of Missouri-Columbia, Biochemistry

Human tissue inhibitors of metalloproteinases (TIMPs) slow tumor growth and slow the development of the blood vessels required to support tumors. These effects are likely mediated by their inhibition of matrix metalloproteinases (MMPs), which are agents of tissue remodeling by way of hydrolysis of proteins of the extracellular matrix. The relaxation of NMR-detected ^{15}N magnetization is employed to identify amplitudes and timescales of internal motions of the backbone of proteins. The timescales accessible in solution are typically picoseconds to nanoseconds and microseconds to milliseconds. Spin-spin relaxation is sensitive to the latter, slower motions. The spin-spin relaxation of the microsecond to millisecond scale motions can be dramatically enhanced by increasing the magnetic field. ^{15}N, T1, T2, and $^{15}N\{^1H\}$NOE measurements of human N-TIMP-1 were collected on the NHMFL 720 MHz NMR spectrometer in November 1999. The 720 MHz data helped confirm Missouri's 500 MHz evidence for microsecond to millisecond motions. The sites of these motions (see Fig. 1) lie at or near the sites of MMP-dependent conformational change in the MMP-binding ridge of N-TIMP-1 seen in its NMR structure.[1,2]

In the year 2000, 720 MHz NMR time has been used to help launch characterization of the catalytic fragment of human MMP-3 when it is bound up by N-TIMP-1. These data have been used to help identify the NMR peaks of the backbone of MMP-3 in this complex. This groundwork will help enable docking of the NMR structure of N-TIMP-1 (see Fig. 2, right section)[1] with the crystal structure of MMP-3,[3] (Fig. 2, left section),[3] using NMR data in water solution. The groundwork will also facilitate studies of the backbone motions of N-TIMP-1 in the complex. Comparison of N-TIMP-1 motions free and bound to the MMP may enhance understanding of the tight binding of these two partners important in human disease and health.

[1] Wu, B., *et al*., Journal of Molecular Biology, **295**, 257-268 (2000).
[2] Gao, G., *et al.,* Journal of Molecular Biology, **301**, 537-552 (2000).
[3] Gomis-Ruth, *et al.,* Nature, **389,** 77 (1997).

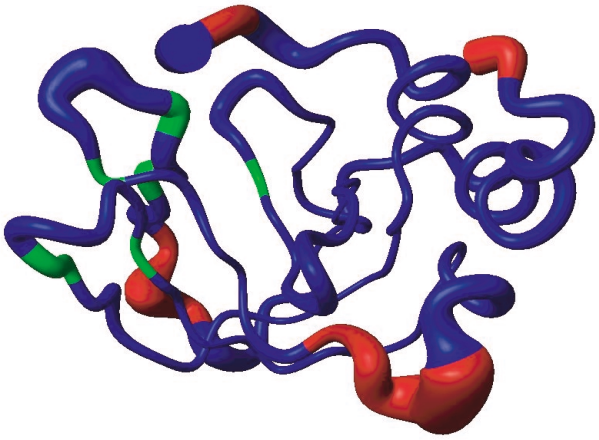

Figure 1. Human TIMP-1 protein backbone plot. Sites of motions in microseconds to milliseconds are in the three hairpin loops at upper left. The leftmost two loops change shape when the MMP-3 binds.

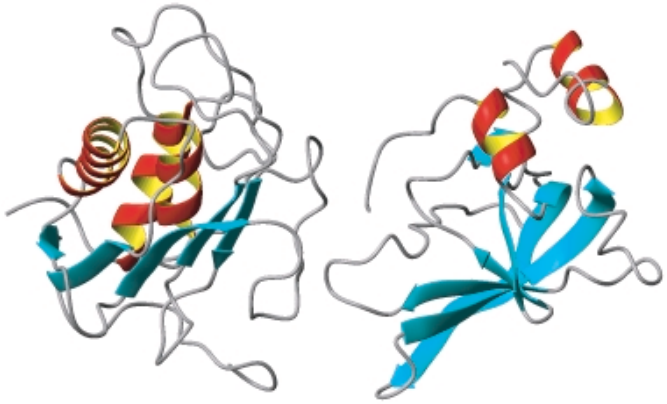

Figure 2. The X-ray model of the catalytic domain of human MMP-3 is at left and the NMR model of human TIMP-1 is at right. Use of NMR to dock these two structures is in progress.

Membrane Protein Structure Determination Using PISA Wheels

Wang, J., NHMFL/FSU, Molecular Biophysics
Kim, S., NHMFL/FSU, Molecular Biophysics
Kovacs, F., NHMFL/FSU, Molecular Biophysics
Cross, T.A., NHMFL/FSU, Chemistry

Patterns of resonances have been recognized in solid state NMR spectra of uniformly aligned samples of alpha-helical membrane proteins. These patterns reflect helical wheels in which it is illustrated that 3.6 amino acid residues complete a full turn of the helix. In the PISA (polar index slant angle) wheel,[1] displayed in the NMR spectra, there are 3.6 resonances per repeat of the circular pattern. The shape, size, and position of these patterns within the spectra reflect the tilt or slant angle of the helix with respect to the bilayer normal that is aligned parallel to magnetic field. This information can be obtained without any resonance assignments. Recognition and characterization of protein structure directly from NMR spectra has not been achieved previously.

The rotational orientation of the helix can be assessed from a single resonance assignment in the helix. In other words, instead of assigning the 20 amide ^{15}N resonances along the entire length of a transmembrane helix, it is possible to make this characterization with a single assignment. Resonance assignments often stand in the way of structure characterization by NMR because of the difficulty in making definitive assignments. However, a few assignments can be readily achieved through an amino acid specific labeling procedure. In other words, all of the isoleucine residues can be ^{15}N labeled at the same time.

In the transmembrane helix of M2 protein, there are five isoleucines at positions 32, 33, 35, 39, and 42. These have been labeled as shown in Fig. 1, and their resonances are resolved. Experimental values of the rotational angle can be assigned to each resonance, and in Fig. 2, these experimental rho values are correlated with predicted rho values from a helical wheel. Residue 33 and resonance e are unique resulting in an unambiguous assignment. Indeed, the rest of the assignments can also be accurately made for the other four isoleucine residues. This assignment uniquely fixes the rotational orientation of the helix within the lipid bilayer. Indeed, with this information, it has been possible to determine at high precision the backbone structure of this transmembrane helix in a hydrated model membrane environment.

Today, there is great interest in high through-put structural characterization. These results suggest that solid state NMR may be able to perform such a task for the third of all proteins that are membrane bound.

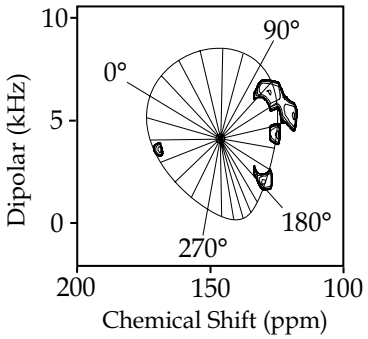

Site	Exp ρ
Ile a	110°
Ile b	130°
Ile c	142°
Ile d	177°
Ile e	323°

Figure 1. Five-site isoleucine labeled transmembrane peptide from the M2 protein of Influenza A virus. The solid state NMR PISEMA spectrum correlates the anisotropic N-H dipolar interaction with chemical shift interaction. The pattern of resonances fit a PISA wheel description as shown, and the rotational orientation angle for each resonance can be quantified.

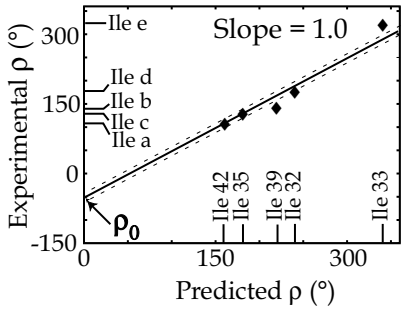

Site	Pre ρ	Assign
Ile 32	240°	Ile d
Ile 33	340°	Ile e
Ile 35	180°	Ile b
Ile 39	220°	Ile c
Ile 42	160°	Ile a

ρ_0 (27–43)=–50°±10°

Figure 2. The experimental rho values are correlated with predicted values from a helical wheel. The line is restricted to a slope of 1.0, resulting in a unique correlation and a sequence specific assignment of the resonances.

[1] Wang, J., *et al.,* J. Magn. Reson., **144**, 162-167 (2000).

Solution Structure of a Prokaryotic SH3 Domain from Diphtheria Toxin Repressor

Wylie, G.W., FSU, Chemistry
Fortune, M., FSU, Chemistry
Logan, T.M., FSU, Chemistry

Diphtheria Toxin Repressor (DtxR) is the best characterized member of a family of proteins that regulate iron uptake in Gram positive bacteria. DtxR is a two domain protein, the N-terminal domain being the better characterized of the two domains in terms of structure and biology. This domain contains two metal binding sites, a DNA binding site, and a dimer interface. We previously determined a three dimensional structure for the C-terminal domain using multidimensional NMR, but a functional role for this domain in repressor activity is not completely clear.

Our previous work with the C-terminal domain involved residues 130-226 of DtxR. This domain was composed of 5 anti-parallel β-strands and three helices. The overall fold is structurally homologous to eukaryotic SH3 domains, which is surprising given the lack of sequence homology between these two domains. We also demonstrated this domain's ability to bind a short peptide sequence that corresponds to residues 125-139 of the full length sequence, but more detailed structural and biophysical studies on peptide binding by this prokaryotic SH3 domain were hampered by intermolecular association in solution in the DtxR(130-226) construct.

Our current work is now with a shorter construct of the C-terminal domain of DtxR from residues 144-226, which lacks the Pro-rich region around residue 130 in the previous construct. This shorter construct doesn't exhibit intermolecular oligomerization, and is a suitable substrate for further studies of the C-terminal domain chemistry and biology. We have used multidimensional heteronuclear NMR spectroscopy to obtain complete backbone and sidechain chemical shift assignments for this construct. We have used these assignments to obtain a set of structural restraints as inputs for structure refinement. Our preliminary structures show that the structure of DtxR(144-226) is very similar to that observed for the longer construct. We will use this structure of DtxR(144-226) as a starting point to investigate the structure of a complex formed between the prokaryotic SH3 domain and a proline-rich peptide.